SPECIAL ISSUE ARTICLE

The Anatomical Record
Advances in Integrative Anatomy and Evolutionary Biology   WILEY

Giant dwarf crocodiles from the Miocene of Kenya and crocodylid faunal dynamics in the late Cenozoic of East Africa

Christopher A. Brochu[1] [ORCID] | Ane de Celis[2] | Amanda J. Adams[1,3] |
Stephanie K. Drumheller[4] | Jennifer H. Nestler[1] | Brenda R. Benefit[5] |
Aryeh Grossman[6,7,8] | Francis Kirera[9] | Thomas Lehmann[10] |
Cynthia Liutkus-Pierce[11] | Fredrick K. Manthi[12] | Monte L. McCrossin[5] |
Kieran P. McNulty[13] | Rose Nyaboke Juma[12]

[1]Department of Earth and Environmental Sciences, University of Iowa, Iowa City, Iowa, USA

[2]Grupo de Biología Evolutiva, Facultad de Ciencias, Universidad Nacional de Educación a Distancia, Madrid, Spain

[3]Department of Biological Sciences, Fort Hays State University, Hays, Kansas, USA

[4]Department of Earth and Planetary Sciences, University of Tennessee, Knoxville, Tennessee, USA

[5]Department of Anthropology, New Mexico State University, Las Cruces, New Mexico, USA

[6]Department of Anatomy, College of Graduate Studies, Midwestern University, Glendale, Arizona, USA

[7]Arizona College of Veterinary Medicine, Midwestern University, Glendale, Arizona, USA

[8]Arizona College of Osteopathic Medicine, Midwestern University, Glendale, Arizona, USA

[9]Mercer University School of Medicine, Macon, Georgia, USA

[10]Senckenberg Research Institute and Natural History Museum Frankfurt, Frankfurt am Main, Germany

[11]Department of Geological and Environmental Sciences, Appalachian State University, Boone, North Carolina, USA

[12]Department of Earth Sciences, National Museums of Kenya, Nairobi, Kenya

[13]Department of Anthropology, University of Minnesota, Minneapolis, Minnesota, USA

Correspondence
Christopher A. Brochu, Department of Earth and Environmental Sciences, University of Iowa, Iowa City, IA 52242, USA.
Email: chris-brochu@uiowa.edu

Abstract

We describe two new osteolaemine crocodylids from the Early and early Middle Miocene of Kenya: *Kinyang mabokoensis* tax. nov. (Maboko, 15 Ma) and *Kinyang tchernovi* tax. nov. (Karungu and Loperot, 18 Ma). Additional material referable to *Kinyang* is known from Chianda and Moruorot. The skull was broad and dorsoventrally deep, and the genus can be diagnosed based on the combined presence of a partial overbite, a subdivided fossa for the lateral collateral ligament on the surangular, and a maxilla with no more than 13 alveoli. Phylogenetic analyses based on morphological and combined morphological and molecular data support a referral of *Kinyang* to Osteolaeminae, and morphological data alone put the new taxon at the base of Euthecodontini. Some *Kinyang* maxillae preserve blind pits on the medial caviconchal recess

wall. *Kinyang* co-occurs with the osteolaemine *Brochuchus* at some localities, and together, they reinforce the phylogenetic disparity between early Neogene osteolaemine-dominated faunas and faunas dominated by crocodylines beginning in the Late Miocene in the Kenya Rift. The causes of this turnover remain unclear, though changes in prevailing vegetation resulting from tectonic and climatic drivers may provide a partial explanation.

KEYWORDS

Africa, Crocodylia, Crocodylidae, Osteolaeminae, paleoecology, phylogenetics

1 | INTRODUCTION

Crocodiles are commonly found in late Cenozoic deposits throughout the East African Rift Valley System (EARS), but most of what we know comes from units no older than about 7 Ma in the Turkana Basin of Kenya and Ethiopia. From that point through the Pliocene and Pleistocene, we see diverse crocodylian faunas dominated by *Crocodylus* Laurenti, 1768 (Figure 1f,g) and the tubulirostrine osteolaemine *Euthecodon* Fourtau, 1920 (Figure 1i; Arambourg, 1947; Azzarà et al., 2021; Brochu, 2020; Brochu & Storrs, 2012; Brochu et al., 2010; Harris et al., 2003; Joleaud, 1930; Storrs, 2003; Tchernov, 1986). Sharp-nosed crocodiles (*Mecistops*
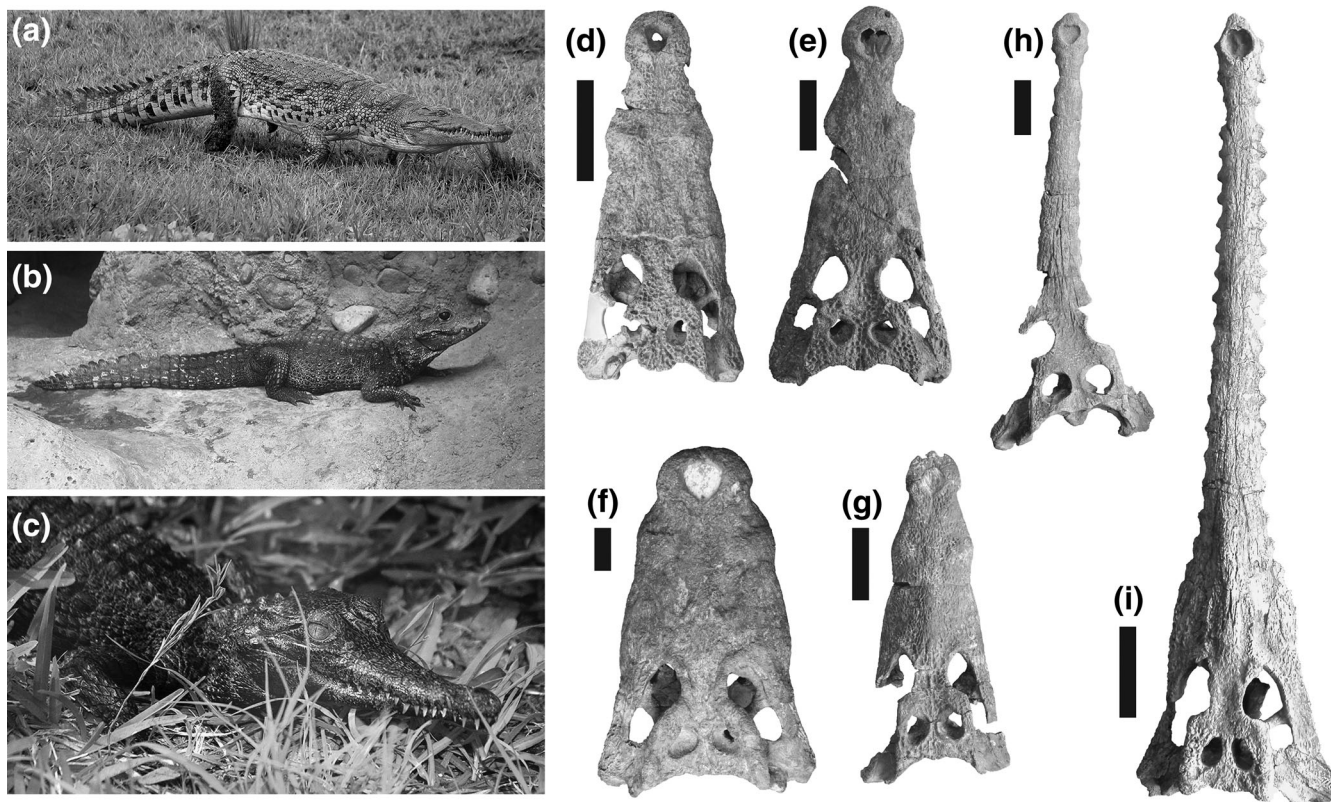
FIGURE 1 Living and extinct crocodylians from the late Cenozoic of East Africa. (a) *Crocodylus niloticus* (Neoafrican *Crocodylus*), Murchison Falls National Park, Uganda. (b) *Osteolaemus tetraspis* (osteolaemine), Lincoln Park Zoo, Chicago, IL, USA. (c) *Mecistops cataphractus* (relationships debated), St. Augustine Alligator Farm, St. Augustine, FL, USA. (d) NHMUK PV R 7729, holotype, *Brochuchus pigotti* (osteolaemine), Rusinga Island, Kenya, early Miocene. (e) KNM LT 23104, *Mecistops* sp., Lothagam, Kenya, late Miocene. (f) KNM ER 1683, holotype, *Crocodylus thorbjarnarsoni* (Paleoafrican *Crocodylus*), Koobi Fora, Kenya, Pleistocene. (g) KNM LT 23108, cf. *Crocodylus checchiai* (crocodyline), Lothagam, Kenya, late Miocene. (h) KNM LT 22943, holotype, "*Eogavialis*" *andrewsi* (gharial), Lothagam, Kenya, late Miocene. (i) KNM ER 1773, *Euthecodon brumpti* (osteolaemine), Koobi Fora, Kenya, Pleistocene. Scale bar = 10 cm (page width)

Gray, 1844) and gharials are also present in the Late Miocene of the region (Figure 1e,h; Adams, 2020; Storrs, 2003), though in smaller numbers.

Less is known about Early or Middle Miocene crocodiles in the EARS. *Euthecodon* (Buffetaut, 1979; Tchernov & Couvering, 1978) and gharials referred by Storrs (2003) to *Eogavialis* Buffetaut, 1982 (Figure 1h) have been reported from sites near Lake Victoria and Lake Turkana, but otherwise, the crocodylian faunas appear to have been very different from those at higher stratigraphic levels. The only crocodylian not sporting a tubelike snout thus far reported from this interval is the small osteolaemine *Brochuchus* Conrad et al., 2013 (Figure 1d), which is unrelated to any generalized crocodylid found later in the Neogene and may not have exceeded 2.5 m in total length (Conrad et al., 2013; Cossette et al., 2020; Tchernov & Couvering, 1978). Nothing ecologically equivalent to large *Crocodylus* has previously been reported.

There thus appears to have been a fundamental shift in the diversity, phylogenetic identity, and ecology of the crocodiles found at either end of the Miocene in the EARS. Tubulirostrine *Euthecodon* and gharials persist, but small flat-snouted osteolaemines are replaced by *Crocodylus* (Figure 1f), some of which were gigantic, with exceptional individuals possibly exceeding 7 m in total length (Brochu & Storrs, 2012).

These changes broadly correlate with several events that impacted East African environments. One of these is the end of the Miocene Climatic Optimum at around 15 Ma (Westerhold et al., 2020), which led to a drop in global mean annual temperatures, a decline in the amount of CO_2 in the atmosphere, and increasingly dry conditions in East Africa. These, in turn, are thought to have led to diminishing woodlands and expansion of C_4 plants (e.g., Feakins et al., 2013; Jacobs et al., 2010; Linder, 2017; Saarinen et al., 2020). This prompted Cossette et al. (2020) to suggest that changes in crocodylian faunas might have reflected changes in vegetation; modern African dwarf crocodiles (*Osteolaemus* Cope, 1861; Figure 1b) are generally limited to forested wetlands (Amoah et al., 2021; Eaton, 2010; Kofron, 1992; Leaché et al., 2006; Riley & Huchzermeyer, 1999; Smolensky, 2015; Waitkuwait, 1986).

But this suggestion was dampened by comparatively weak sampling in Early to Middle Miocene units and the co-occurrence of regional tectonic effects, including changes in topography and river drainage, the appearance of deep graben-fill lakes like Lake Turkana, and volcanic events related to the opening of the Rift Valley itself (e.g., Bergner et al., 2009; Chorowicz, 2005; Feibel, 2011; Rooney, 2020; Wichura et al., 2015). More information is needed about Miocene crocodylians in East Africa to understand the causes of this turnover.

Here, we describe a new genus of osteolaemine crocodile from Early and early Middle Miocene sites in the Turkana and Lake Victoria Basins in Kenya (hereafter TB and LVB; Figure 2). At least two diagnosable species can be recognized—one from Maboko Island in Lake Victoria dating to approximately 15 Ma, and another from Loperot (TB) and Karungu (LVB) dating to approximately 18 Ma. Some of the specimens preserve unexpected derived states, especially within the rostrum, that suggest higher levels of homoplasy and intraspecific variation for some of the characters used to reconstruct crocodylid phylogeny than previously anticipated. Although not unusually large for a crocodylid, they are substantially larger than *Brochuchus*, which is known from some of the same sites, and they are larger still than their closest living relatives, diminutive *Osteolaemus*. The cranial proportions of the new species differ from those of any extant crocodylid. They thus reinforce the stark morphological, phylogenetic, and presumably ecological contrasts between older and younger Neogene crocodylian faunas in East Africa.

1.1 | Institutional abbreviations

AMNH, American Museum of Natural History, New York, United States; *BRSUG*, Department of Earth Sciences, University of Bristol, United Kingdom; *FMNH*, Field Museum of Natural History, Chicago, IL, United States; *KNM*, National Museums of Kenya, Nairobi; *NHMUK*, Natural History Museum, London, United Kingdom; *SUI*, Paleontological Repository, University of Iowa, Iowa City, United States; *UFMNH*, University of Florida Museum of Natural History, Gainesville, United States; *USNM*, United States National Museum of Natural History, Smithsonian Institution, Washington, DC, United States.

1.2 | Anatomical abbreviations

Alveolar/tooth positions will be indicated with a letter indicating the bone on which they appear (p for premaxilla, m for maxilla, d for dentary) and a number indicating position in the tooth row from mesial to distal. The fourth maxillary tooth posterior to the premaxilla would thus be m4, for example.

Abbreviations ending in "ss" indicate sutural surfaces for the angular (*anss*), articular (*arss*), ectopterygoid (*ectss*), (*fss*), jugal (*jss*), lacrimal (*lss*), maxilla (*mxss*), nasal (*nss*), palatine (*palss*), parietal (*pass*), prefrontal
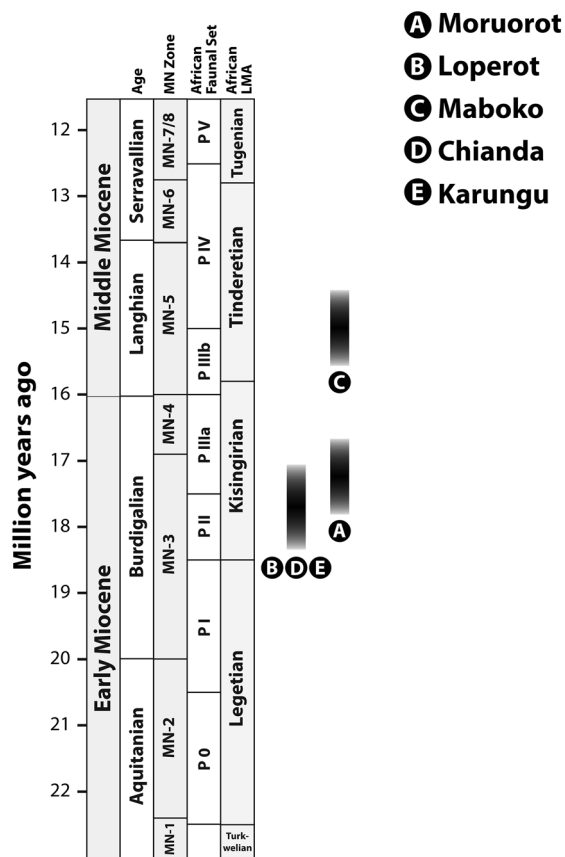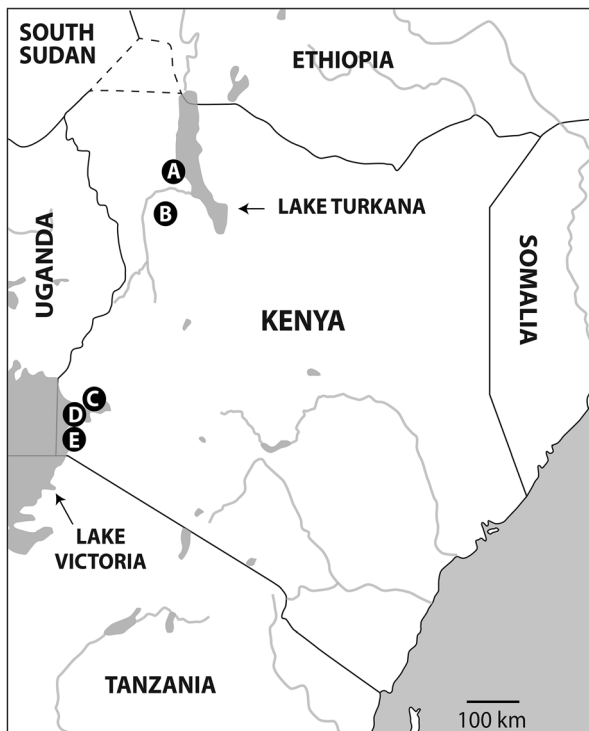
FIGURE 2 Spatiotemporal positions of sites discussed in this article. Columns in lower figure include European Neogene Mammal (MN) Zones, African Faunal Sets proposed by Pickford (1981, 1983), and African Land Mammal Ages proposed by Van Couvering and Delson (2020) (column width)

(*prss*), premaxilla (*pmss*), splenial (*spss*), and postorbital (*poss*).

an, angular; *ans*, axis neural spine; *ar*, articular; *bo*, basioccipital; *bp*, blind pit on caviconchal recess medial wall; *bs*, basisphenoid; *cc*, circumchoanal crest; *ccr*, caviconchal recess medial wall; *ch*, choana; *co*, coronoid; *cof*, coronoid foramen; *d*, dentary; *dpc*, deltopectoral crest; *dss*, dentary symphyseal surface; *ect*, ectopterygoid; *emf*, external mandibular fenestra; *en*, external naris; *eo*, exoccipital; *eor*, external otic recess; *f*, frontal; *fae*, foramen aëreum; *fic*, foramen intermandibularis caudalis; *fim*, foramen intermandibularis medius; *fm*, foramen magnum; *gf*, glenoid fossa; *h*, hypophysis; *if*, incisive foramen; *itf*, infratemporal fenestra; *j*, jugal; *l*, lacrimal; *lcf*, lateral carotid foramen; *lclf*, fossa for lateral collateral ligament; *leu*, lateral eustachian foramen; *lf*, lingual foramen on surangular; *lsc*, lateral surangular crest; *lsg*, lateral squamosal groove; *meu*, median eustachian foramen; *mg*, Meckelian groove; *mx*, maxilla; *mcs*, midchoanal septum; *n*, nasal; *npdm*, mold of nasopharyngeal duct; *oc*, occipital condyle; *od*, odontoid; *op*, occlusal pit; *or*, orbit; *p*, parietal; *pal*, palatine; *pf*, prefrontal; *pfp*, prefrontal pillar; *pmx*, premaxilla; *pnr*, prenarial rostrum; *po*, postorbital; *pob*, postorbital bar; *poz*, postzygapophysis; *pp*, palatine process; *pt*, pterygoid; *ptf*, posttemporal fenestra; *q*, quadrate; *qj*, quadratojugal; *qlh*, quadrate lateral hemicondyle; *qmh*, quadrate medial hemicondyle; *rap*, retroarticular process; *sa*, surangular; *sal*, ascending lamina of surangular; *so*, supraoccipital; *sof*, suborbital fenestra; *sp*, splenial; *sq*, squamosal; *stf*, supratemporal fenestra; *vf*, vagus foramen; *xii*, foramen for 12th cranial (hypoglossal) nerve.

1.3 | Taxonomic notes

We use the phylogenetic definitions formulated by Brochu (2003), with Crocodylidae applied in the molecular context (last common ancestor of *Osteolaemus tetraspis* Cope, 1861 and *Crocodylus niloticus* and all of its descendants. This does not impact the taxonomic status of *Kinyang*, which would be a member of Crocodylidae regardless of context, but it does bear on more rootwardly located species such as *Prodiplocynodon langi* Mook, 1941 or "*Crocodylus*" *affinis* Marsh, 1871; these were treated as crocodyloids under the morphological context, but are here called "stem longirostrines."

Cossette et al. (2020) applied the term "Paleoafrican *Crocodylus*" to an assemblage including extinct *Crocodylus thorbjarnarsoni* Brochu and Storrs, 2012 (Figure 1f) and *C. anthropophagus* Brochu et al., 2010. The two living species of *Crocodylus* found in Africa

(*C. niloticus* and *C. suchus*; Figure 1a) were called Neoafrican *Crocodylus*. These are informal terms, and Neoafrican *Crocodylus* may not be monophyletic (e.g., Hekkala et al., 2011). We continue this practice here. Paleoafrican *Crocodylus* does not include fossils referred to *Crocodylus checchiai* Maccagno, 1947 from the Late Miocene of Kenya by Brochu and Storrs (2012); the results of analyses in this article would support inclusion, but other analyses do not (e.g., Brochu & Storrs, 2012; Cossette et al., 2020; Delfino et al., 2020).

2 | SYSTEMATIC HIERARCHY

Crocodylia Gmelin, 1789 (sensu Benton & Clark, 1988)

Crocodylidae Gray, 1825 (sensu Brochu, 2003, independent of context)

Osteolaeminae Brochu 2003

2.1 | *Kinyang*, tax. nov.

2.1.1 | Type species

Kinyang mabokoensis Brochu et al. (this publication).

2.1.2 | Etymology

Kinyang is based on words for "crocodile" in the Nilotic languages spoken where these fossils have been found in northern and western Kenya, such as *akinyang* (Turkana), *nyang* (Dholuo), *kinio* (Bari), *lkinyang* (Samburu), and *lkinian* (Maa).

2.1.3 | Diagnosis

Crocodylid with robust skull and broad, deep rostrum. Shares a linear frontoparietal suture with *Osteolaemus*; *Voay* Brochu, 2007; *Rimasuchus* Storrs, 2003; *Brochuchus* Conrad et al., 2013; and "*Crocodylus*" *gariepensis* Pickford, 2003. Shares forked or cleft maxillary ectopterygoid ramus with *Crocodylus* and *Brochuchus*. Dorsal lamina of surangular adjacent to glenoid fossa truncated. Quadratojugal extends to, or almost to, dorsal corner of infratemporal fenestra. Plesiomorphic dental occlusion pattern with deep occlusal pits between the sixth through eighth maxillary teeth, but an overbite otherwise. Ectopterygoid forms broad shelf medial to maxillary toothrow. Lateral margins of palatine process oriented anteromedially, but process does not terminate

in acute point. Fossa on surangular for lateral collateral ligament subdivided; 12 or 13 maxillary alveoli.

2.2 | *Kinyang mabokoensis*, sp. nov.

2.2.1 | Holotype

KNM-MB 29176, skull and jaws (Figures 3, 4, 5a, and 6).

2.2.2 | Referred material

KNM-MB 21977, left articular (Figure 7p); KNM-MB 25727, partial right squamosal (Figure 7I,j); KNM-MB 25729, partial left postorbital; KNM-MB 25747, frontal; KNM-MB 25748, right nasal (Figure 7f); KNM-MB 25749, left premaxilla (Figures 7c–e and 7a); KNM-MB 25752, frontal (Figure 7g); KNM-MB 25756, partial left surangular (Figure 7k,l); KNM-MB 25757, right maxilla (Figure 7a,b); KNM-MB 28136, right prefrontal (Figure 7h); KNM-MB 28143, left dentary (Figure 7m–o); KNM-MB 83205, right articular. KNM-MB 25747, 25748, and 25749 might be associated.

2.2.3 | Occurrence

Middle Miocene Maboko Formation, Maboko Island, Kenya (Figure 2). All identified specimens were excavated and mapped in place within in situ Bed 3 sediments at Maboko Main (Benefit, 1999; Benefit & McCrossin, 1989). All were found just above the undulating surface of Bed 2 bentonite, which underlies Bed 3. Ooids and oncoids in Bed 3 sediment collected in direct association with the type specimen, as well as topographic features, indicate deposition in a low energy freshwater environment that appears to have been the beach ramp of a lake of unknown size and depth (Watkins, 2004). Isotopic analysis of mammalian herbivore enamel from Bed 3 indicates an open forest/woodland vegetation close to the site of deposition, as well as the absence of C4 grasses (Arney et al., In review; Arney et al., 2018). Since analysis of microwear and macrowear on Maboko gomphotheriid proboscidean enamel indicates grass-dominated mixed feeding (Saarinen et al., 2020), C3 grasses must have been present at Maboko. Local fluctuations in water table are indicated by the presence of Bed 4 calcrete above the Bed 3 sandy clay, followed by a later transition to Bed 5 mudstone. Primary and ungulate faunas as well as carbon isotope signatures indicate a more densely wooded environment in the lower portion of Bed 5 (Bed 5b) (Benefit, 1999;
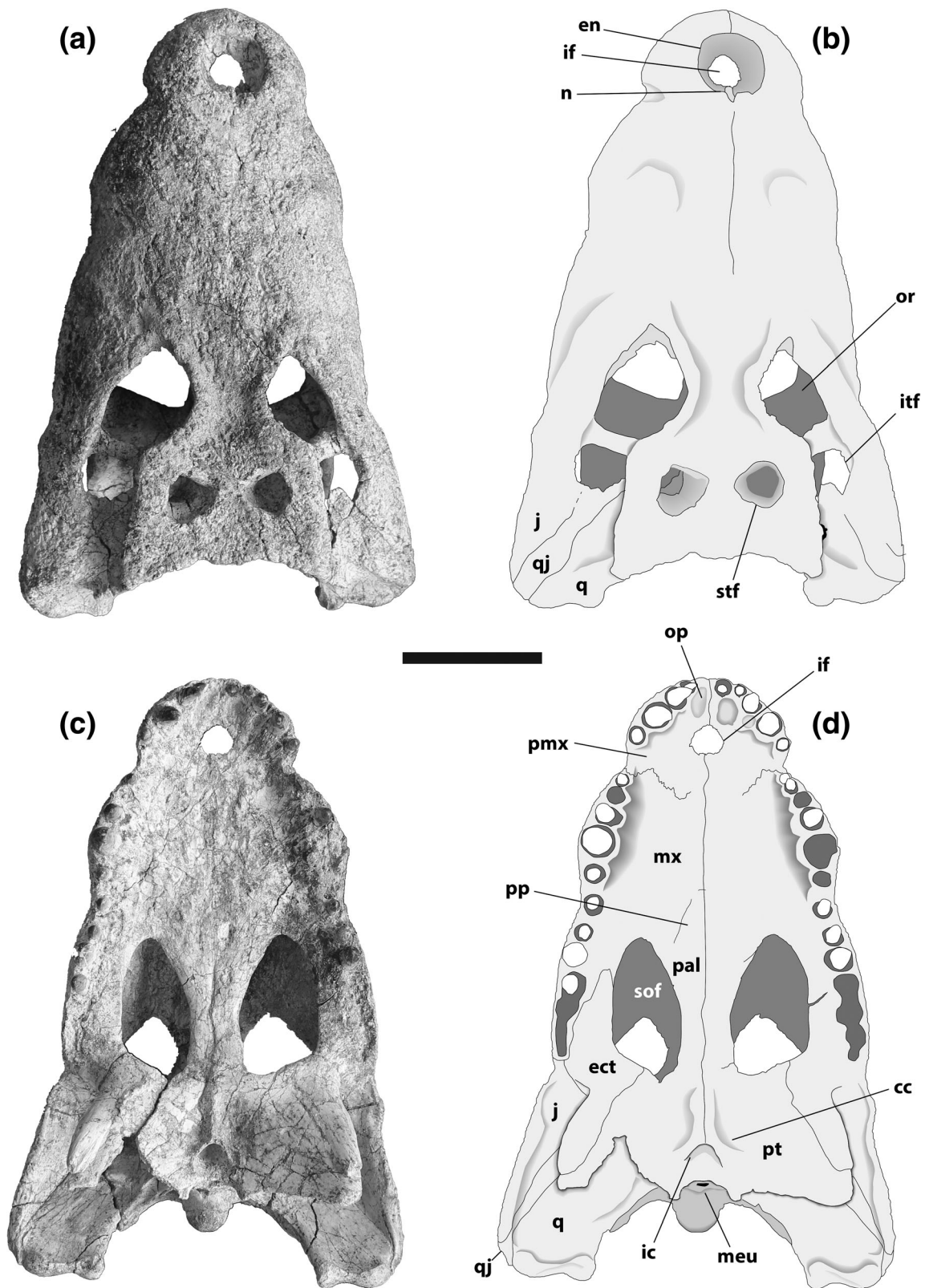
FIGURE 3 KNM-MB 29176, holotype, *Kinyang mabokoensis*, skull, dorsal (a, b) and ventral (c, d) view. Scale = 10 cm (page width)

Retallack et al., 2002). The abundant bird fauna from higher sediments in Bed 5 (5w) include pelicans, storks, cormorants, and flamingos (Mayr, 2014; Retallack et al., 2002) indicative of a transition toward a wetter and possibly more open woodland. Thousands of isolated and unidentifiable crocodile teeth (N = 4,703) and scutes
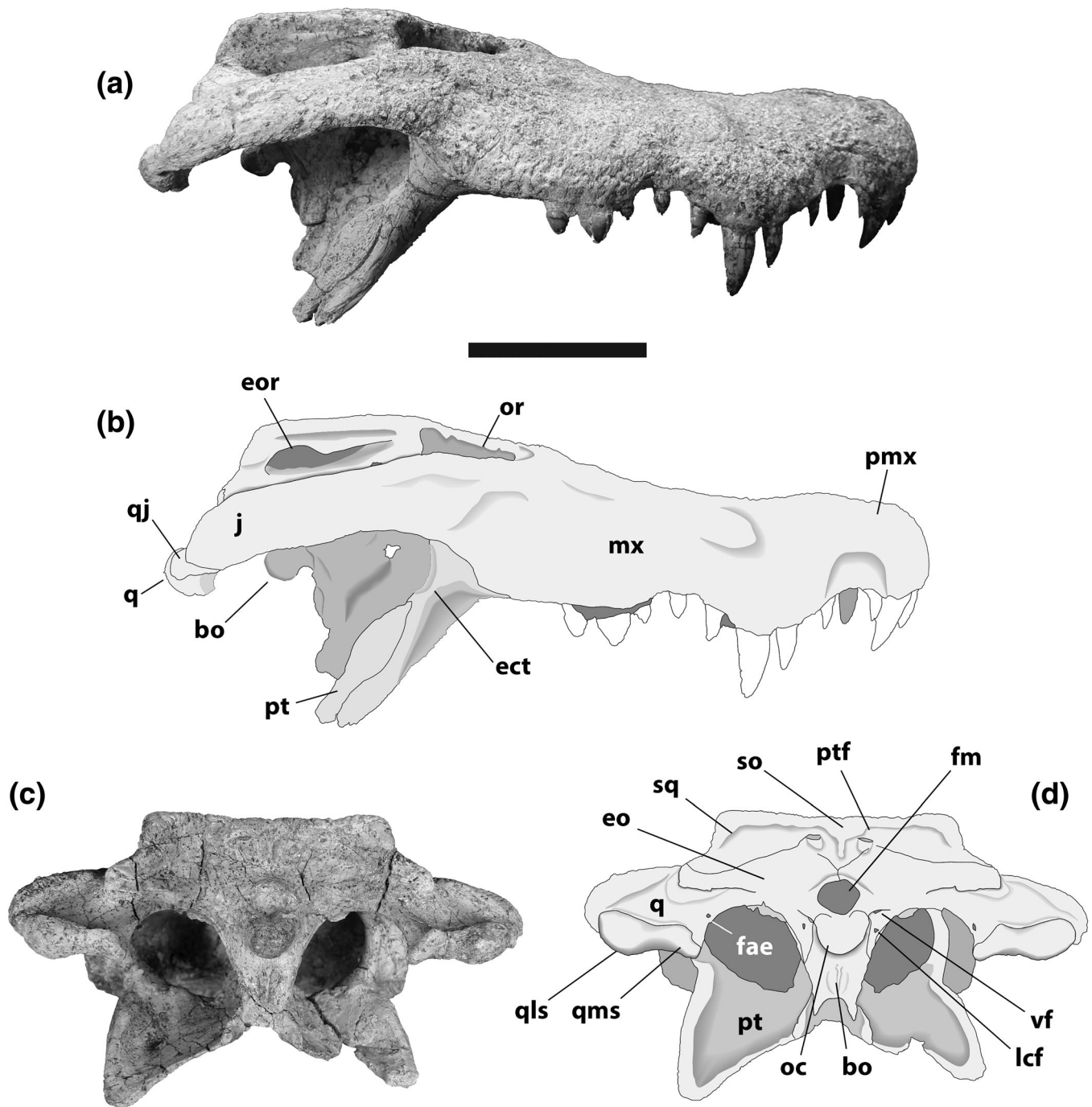
FIGURE 4 KNM-MB 29176, holotype, *Kinyang mabokoensis*, skull, right lateral (a, b) and posterior (c, d) view. Scale = 10 cm. (page width)

($N = 458$) were recovered from a circumscribed 16×16 m² excavated area of 2 m depth within Bed 5. This exceeds the abundance of isolated crocodile remains ($N = 378$ crocodile teeth and $N = 57$ scutes) in a circumscribed area of the same size from Bed 3. Since none of the Bed 5 crocodile fossils are identifiable, we cannot presently confirm whether *K. mabokoensis* and/or the sympatric species *Brochuchus parvidens* survived the localized changes in water table within the Maboko Formation.

^{40}Ar/^{39}Ar dating of the Bed 8 tuff upsection of Bed 3 resulted in a mean age of 15.4 Ma, with the youngest date being 14.7 (Feibel & Brown, 1991). Hence, Bed 3 fossils are older than 14.7 Ma, but radiometric dating of material underlying Bed 2 has yet to be successful. The presence of several mammalian groups (bovids, giraffoids, hippopotamids, derived choerolophodont gomphotheres, and large-bodied kenyapithecine hominoids) that do not occur in the Early Miocene of nearby

Rusinga indicates that Maboko Bed 3 is more recent than 17 Ma and thus Middle Miocene (Andrews et al., 1981; Peppe et al., 2011, 2017; Pickford, 1983; Retallack et al., 2002).

2.2.4 | Etymology

mabokoensis, for Maboko Island, where the holotype was found.

2.2.5 | Diagnosis

Linear array of pits on medial wall of caviconchal recess (Figure 8a; unknown in *Kinyang* from other localities, and shared with extant *Crocodylus*). Suborbital fenestra broad (length-width ratio = 1.83). Naris opens dorsally. Maxillary ramus of ectopterygoid broad, but medial margin linear or only slightly convex.

2.2.6 | Description

The holotype skull (Figures 3 and 4) is nearly complete and undistorted, and the snout is remarkably short and deep for a crocodylid of this size. Unfortunately, very few sutures can be seen on the specimen. Most such information comes from isolated cranial elements.

The external naris is large and projects dorsally, and there is virtually no prenarial rostrum (Figure 5a). An isolated left premaxilla (KNM-MB 25749) strongly suggests that the nasals either did not reach the naris externally or did so as a pair of very thin processes; the midline sutural surface anterior to the naris is very nearly on the same sagittal plane as the sutural surface emerging from the posterior narial margin. A small process within the narial chamber may be an anterior expression of the nasals, suggesting that if they did not contact the naris externally, they passed anteriorly between the premaxillae. The posterior premaxillary process on the dorsal surface extends no further than the third maxillary alveolus (m3), and KNM-MB 25749 (Figure 9d) suggests that the lateral margin of the process was indented. In ventral view, each premaxilla bears five alveoli, the largest of which is the fourth. The incisive foramen is circular and situated near the center of the premaxillary palate. The palatal premaxillary-maxillary sutures are incompletely preserved, but the right suture is clearly convex (Figures 2d and 4e), which would have given the complete suture a W shape.

A right nasal (KNM-MB 25748, Figure 9f) bears a posteromedial indentation, indicating the sutural surface

FIGURE 5 (a) KNM-MB 29176, holotype, *Kinyang mabokoensis*, snout, dorsal view. (b) USNM 194830, *Crocodyus suchus*, snout, dorsal view. Scale = 1 cm (column width)

for the frontal anterior process. Attachment surfaces for the prefrontal and lacrimal are preserved posterolaterally. The lateral and medial surfaces are nearly parallel for most of the length of the nasal, with an anteromedially-oriented surface for contact with the premaxilla. We believe the anterior tip is complete, and that a small chip of bone near the anterior end is a small fragment of the right premaxilla; if this interpretation is correct, the nasal was excluded from the external naris externally.

The palatal lamina of the maxilla is elevated, giving the palate as a whole a vaulted appearance. The number of maxillary teeth is ambiguous, but would have been comparatively low; the holotype suggests 13 alveoli on either side, but the isolated maxilla KNM-MB 25757 (Figure 9a) indicates no more than 12. Maxillary tooth counts in modern crocodylians can vary by one (Brown et al., 2015, and CAB, personal observation), so this is not remarkable. Occlusal pits are absent except between m6 through m8, and these are more lingually placed than in other crocodylids.

KNM-MB 25757 bears a series of blind pits on the medial wall of the caviconchal recess (Figure 8a). These are present from dorsal to m4 to the posterior end of the recess as preserved, and they are especially large and deep dorsal to m5 and m6. This specimen also preserves the sutural surface for the nasal, which forms a deep groove in medial view and convex in dorsal view, suggesting that the nasals may have been constricted between the maxillae.

Little else can be said about the rostrum in dorsal view. There are no prominent rostral crests or bosses, but a modest crest, presumably on the prefrontal, extends anteriorly from the orbital rim. Dorsally, the prefrontal pillar is anteroposteriorly expanded with a thin lateral lamina.

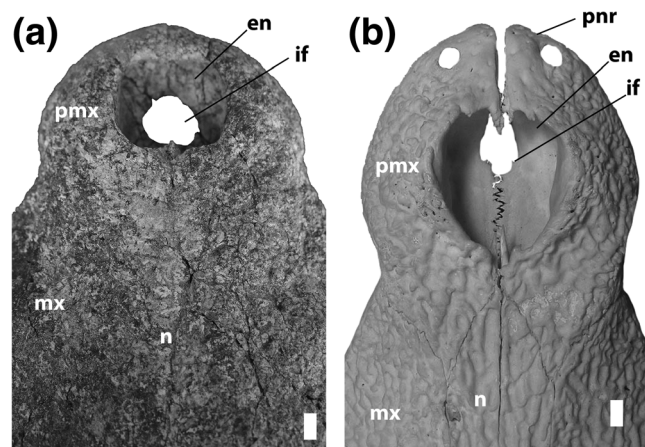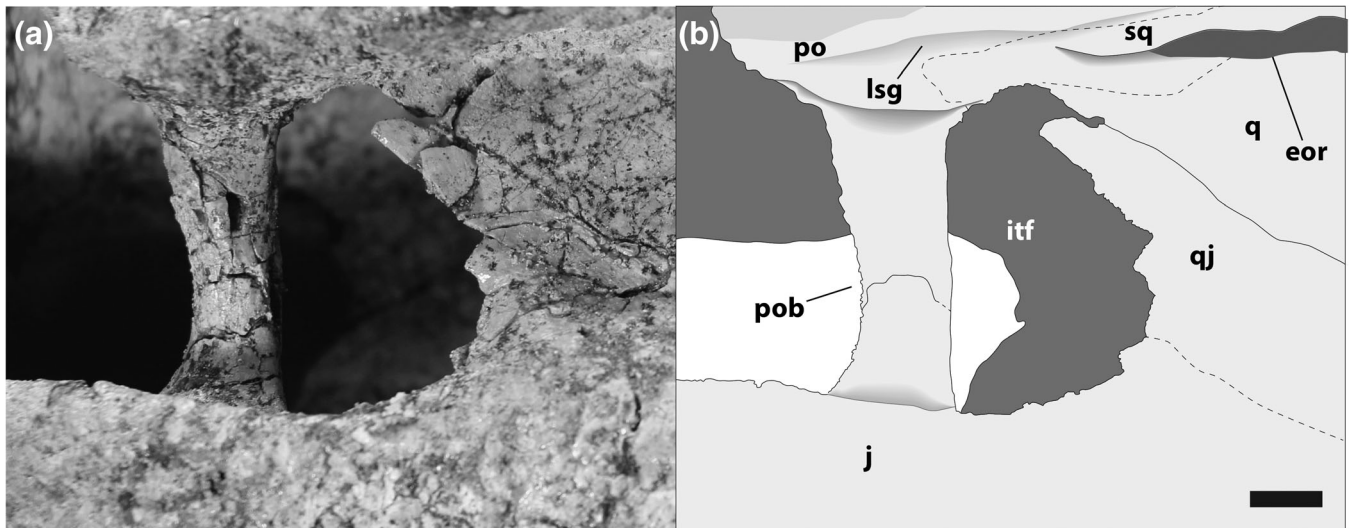**FIGURE 6** (a and b) KNM-MB 29176, holotype, *Kinyang mabokoensis*, left infratemporal fenestra, dorsolateral view. Scale = 1 cm (page width)

The jugal underlying the infratemporal fenestra is flattened. A convexity along its lateral surface, anterolateral to the infratemporal fenestra, bears a shallow ventral fossa.

The medial orbital margin is upturned, and a modest crest extends anteriorly from the orbital rim. The frontal bears a long anterior process, but its anteriormost extent is unclear. Intersection of the frontal-prefrontal suture with the orbit is nearly perpendicular. Sutural contacts with the postorbital and parietal are nearly rectilinear, and the frontoparietal suture is entirely on the skull table.

The postorbital bar is slender and inset from both the skull table and lateral jugal surfaces. The postorbital forms the anterolateral margin of the circular supratemporal fenestra, and the squamosal forms its posterolateral margin. There is a deep, unflared groove on the lateral surface of the dorsally flat skull table. The lateral margins of the skull table are nearly parallel, though they have a slight anteromedial orientation and bear a modest rounded lateral projection dorsal to the otic aperture.

The D-shaped infratemporal fenestra is relatively small. The jugal forms the posteroventral corner, and the quadratojugal extended to, or very near to, the dorsal corner (Figure 6a). Damage to the posterior margin makes it impossible to assess the presence of a quadratojugal spine or a quadrate contribution to the fenestra.

The quadrate rami are short and project posteroventrally. The small foramen aëreum is on the dorsomedial surface of the ramus. The quadratojugal extends nearly to the posterior end of the ramus, and the medial quadrate hemicondyle is dorsally expanded.

The jugal and quadratojugal approach each other closely on the ventral surface before the jugal-quadratojugal and quadratojugal-jugal sutures diverge anteriorly. A thin crest on the ventral surface, merging anteriorly with a boss, represents the attachment surface for the adductor musculature.

The palatines meet at the midline and extend anteriorly forward of the oval suborbital fenestrae. The anterior palatine process has a characteristic shape combining features usually associated with both broad- and slender-snouted crocodyliforms. In most broad-snouted forms, the lateral margins of the process are parallel and the process as a whole is U-shaped. Slender-snouted forms, by contrast, typically have V-shaped processes with anteromedially oriented lateral margins that converge anteriorly at a point. Only the right lateral margin can be seen on the holotype, and it is oriented anteromedially. But the segment of the anterior margin preserved on the specimen is almost linear, strongly suggesting that the process was not V-shaped. The palatines are constricted and flare anteriorly between the suborbital fenestrae, and the palatine-pterygoid contact is anterior to the posterior margins of the fenestrae.

The maxillary ramus of the ectopterygoid is robust and lies adjacent to the posteriormost four or five maxillary alveoli. Although its ventral surface is broad, its medial margin is only modestly convex. It thus does not impart a deep concavity to the outline of the suborbital fenestra. Its anterior tip is deeply cleft, and its sutural surface with the maxilla is deeply inset. The ascending ramus of the ectopterygoid forms the posteroventral part of the postorbital process, and the pterygoidal ramus lies on the ventral surface of the pterygoid wing. The anterior

surface of the pterygoidal ramus, forming the posterior margin of the suborbital fenestra, is flattened, with only a modest convexity in its outline.

The pterygoids remain separate anterior to the internal choana, but are fused posterior to it. Their surfaces are deeply elevated anterolateral to the internal choana, which opens posteroventrally and lacks a septum. The elevated margins form a thin crest that nearly surrounds the choanal aperture (Figure 10a).

The lateral braincase wall is exposed, but sutures are largely obliterated. If there was a sulcus between the basisphenoid rostrum and pterygoids, it was shallow. D-shaped depressions indicate the posterolateral exposure of the basisphenoid, and in both cases they are ventral to the lateral carotid foramen. A thin crest extends on the ventral surface of the quadrate from the base of the quadrate ramus to approximately the ventralmost tip of the exoccipital.

The skull table overhangs the occipital surface in posterior view. The triangular supraoccipital bears a prominent sagittal crest and forms the floors of the small postorbital fenestrae, but whether it was exposed on the skull table dorsally is unknown. There are bosses on the posterior surface of the exoccipitals near the lateral tips of the paroccipital processes. The exoccipitals meet at the midline and preclude the supraoccipital from contributing to the foramen magnum. Foramina for the hypoglossal nerve are not preserved on either side of the foramen magnum, but oval depressions filled with matrix represent the vagus fossae. The lateral carotid foramina are small and circular. The exoccipitals extend along the lateral margins of the basioccipital, but do not reach the basioccipital tubera. The basioccipital forms the occipital condyle and the floor of the foramen magnum. It is broad ventral to the condyle, bearing a sagittal crest and less prominent lateral bosses.

The suture for the basisphenoid itself cannot be traced ventral to the basioccipital, but the morphology of the basioccipital and pterygoid strongly suggests a plesiomorphic arrangement for the eustachian foramina and an extensive basisphenoid exposure. The large medial eustachian foramen is preserved at the ventral tip of the basioccipital. The lateral eustachian openings are not directly preserved, but the ventral surface of the basioccipital is oriented dorsolaterally on either side of the medial foramen. This is inconsistent with a placement of the three eustachian foramina on the same transverse plane. The pterygoid is deep ventral to the medial eustachian foramen, and the posterior processes are dorsoventrally tall. In other crocodylians with this condition, the basisphenoid extends ventrally below the basioccipital and is broadly exposed posterior to the pterygoid. Moreover, V-shaped crests extending ventrolateral to the medial eustachian foramen might represent the lateral margins of the basisphenoid.

Based on the right ramus of the holotype and an isolated left dentary (KNM-MB 28143), there are 15 dentary alveoli. The fourth and eleventh are largest. The small third and much larger fourth are not confluent. There are diastemata, corresponding with notches on the lateral surface of the dentary, between d2 and d3 and between d7 and d9. The dentary symphysis extends to the level of d6. Posteriorly, the dentary forms the anterodorsal margin of the external mandibular fenestra.

The splenials do not meet at the midline (Figure 7e,f). Each terminates anteriorly at the level of the seventh or eighth dentary alveoli, and although it extends further anteriorly ventral to the Meckelian groove than dorsally, the disparity between the dorsal and ventral tips is slight. The splenial expands dorsoventrally from its anterior tip to the level of d11, and it forms the medial margin of the distalmost four or five alveoli. It is imperforate, and its dorsal surface is flattened and medially expanded posteriorly. The foramen intermandibularis medius is not preserved on either side, but the splenial forms the anterodorsal margin of the foramen intermandibularis caudalis (Figure 7I,j). The splenial bears a posterior process between the coronoid and angular dorsal to the foramen intermandibularis caudalis.

Dorsally, the left coronoid of the holotype is well preserved (Figure 7I,j). Its dorsal margin is horizontal and its anterior margin is rounded. It presumably formed the posterior margin of the foramen intermandibularis medius, but the anterior margin is damaged. Its main body is imperforate. A small part of the ventral process along the dorsal rim of the Meckelian fossa is preserved on the right, lapping over the medial surface of the ascending lamina of the angular. The angular extends from its anterior tip level with d14 to the distal tip of the retroarticular process. Laterally, it forms the posteroventral margin of the external mandibular fenestra. There is a sharp discontinuity between its heavily pitted surface adjacent to the dentary and surangular and inset smooth surface where it contacts the articular. In medial view, it forms the posterior and dorsal margins of the foramen intermandibularis caudalis and bears a robust ascending lamina, which forms the medial wall of the Meckelian fossa.

The surangular extends from the dentary toothrow, with a thin spur lying along the medial margin of the last dentary alveolus, to the distalmost tip of the retroarticular process. It bears a pair of anterior processes, the dorsalmost of which is longer than its ventral counterpart. Its dorsal surface is flattened. The pit for the lateral collateral ligament adjacent to the glenoid fossa is subdivided, with a crest splitting it into anterior and posterior subfossae; this subdivision is modest on an isolated surangular (KNM-MB 25756), but prominent on the
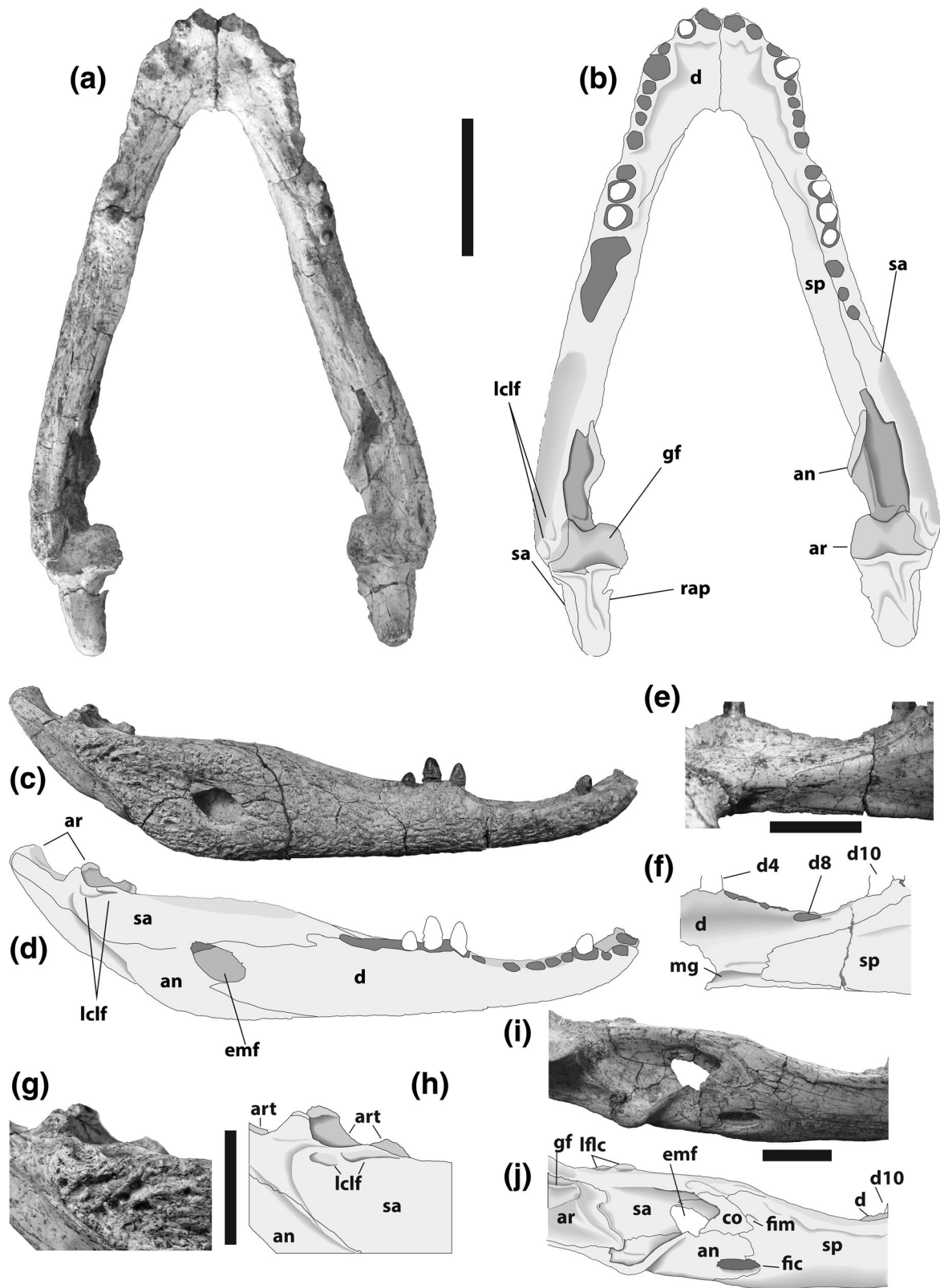
FIGURE 7 KNM-MB 29176, holotype, *Kinyang mabokoensis*, lower jaw, dorsal (a, b) and right lateral (c, d) view. Anterior part of right ramus, medial view (e, f). Articular region of right ramus, lateral view (g, h). Meckelian fossa and surrounding area, left ramus, medial view (i, j). Scale = 10 cm (a–d), 5 cm (e–j) (page width)
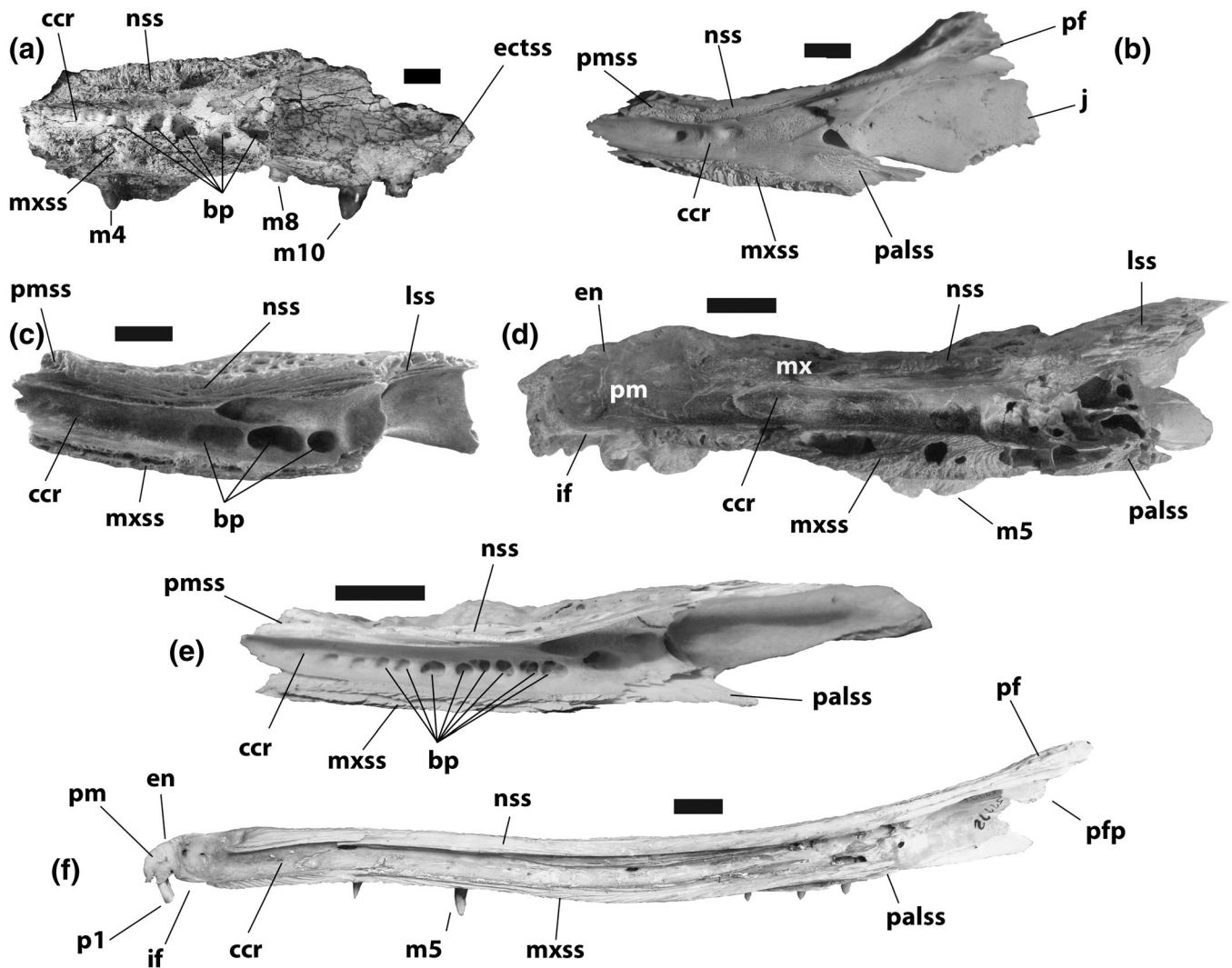
FIGURE 8 Crocodylid right maxillae, medial view. (a) KNM-MB 25757, *Kinyang mabokoensis*. (b) UFLMNH 34784, *Osteolaemus tetraspis* (left maxilla, image reversed). (c) BRSUG 27279, ?*Rimasuchus lloydi*, Gebel Zelten, Libya (left maxilla, image reversed). (d) BRSUG 27275, ?*Rimasuchus lloydi*, Gebel Zelten, Libya. (e) KNM-OR 19, *Crocodylus niloticus*. (f) AMNH R 29300, *Mecistops cataphractus*. Scale = 1 cm. (page width)

holotype (Figure 7g,h). Its suture with the articular within the glenoid fossa is bowed, and although it bears a dorsal process adjacent to the posterior wall of the glenoid fossa, the process is truncated and does not extend to the dorsal rim. Its posteriormost tip is rounded. Laterally, it forms the dorsal and part of the posterior edge of the external mandibular fenestra, but the surangular-angular suture appears to intersect the fenestra at its posteriormost end and not to pass ventrally and anteriorly along the fenestral margin.

The glenoid fossa of the articular bears two subfossae, one for each of the quadrate hemicondyles. The posterior rim of the fossa is expanded dorsally. The foramen aëreum was very small and located on the medialmost corner of the posterior glenoid fossa rim. The main articular body bears a thin anterior lamina on the medial

surface of the surangular dorsal to the lingual foramen, which lies on the articular-surangular suture. The retroarticular process projects posterodorsally and bears a broad dorsal midline crest.

Postcranial crocodylian material is known from Maboko. All of it comes from comparatively small animals. Because the small crocodylid *Brochuchus* is also known from Maboko (Cossette et al., 2020), it is not possible to refer any of it to either species.

2.3 | *Kinyang tchernovi,* sp. nov.

2.3.1 | Holotype

KNM-LP 69374, partial skull (Figure 11).
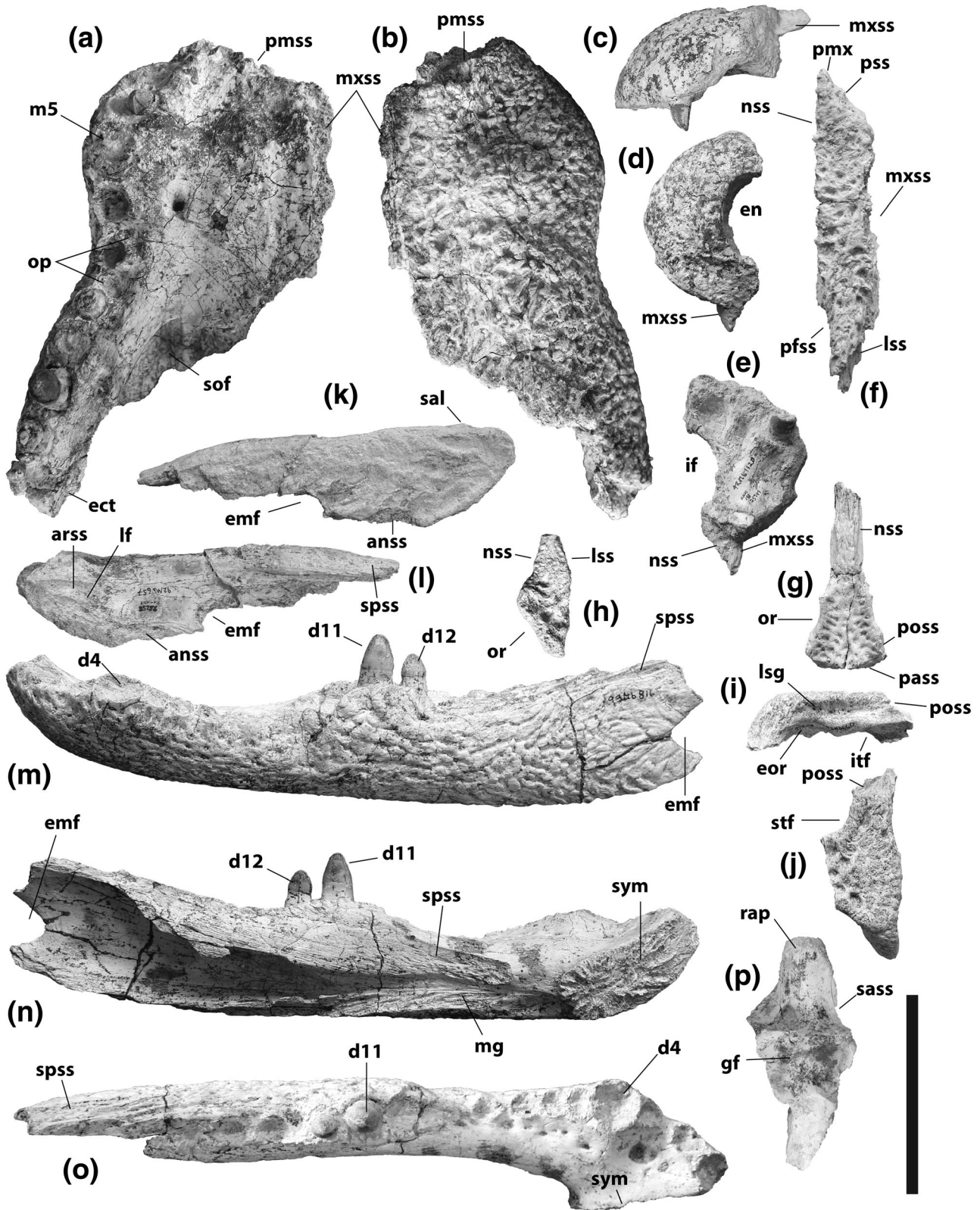
FIGURE 9 Isolated craniomandibular remains referred to *Kinyang mabokoensis*. NM-MB 25757, right maxilla, ventral (a) and dorsal (b) view. KNM-MB 25749, left premaxilla in lateral (c), dorsal (d), and ventral (e) view. KNM-MB 25748, right nasal, dorsal view (f). KNM-MB 25752, frontal, dorsal view (g). KNM-MB 28136, right prefrontal, dorsal view (h). KNM-MB 25727, partial right squamosal, lateral (i) and dorsal (j) view. KNM-MB 25756, partial left surangular, lateral (k) and medial (l) view. KNM-MB 28143, left dentary, lateral (m), medial (n), and dorsal (o) view. KNM-MB 21977, left articular, dorsal view (p). Scale = 10 cm (page width)
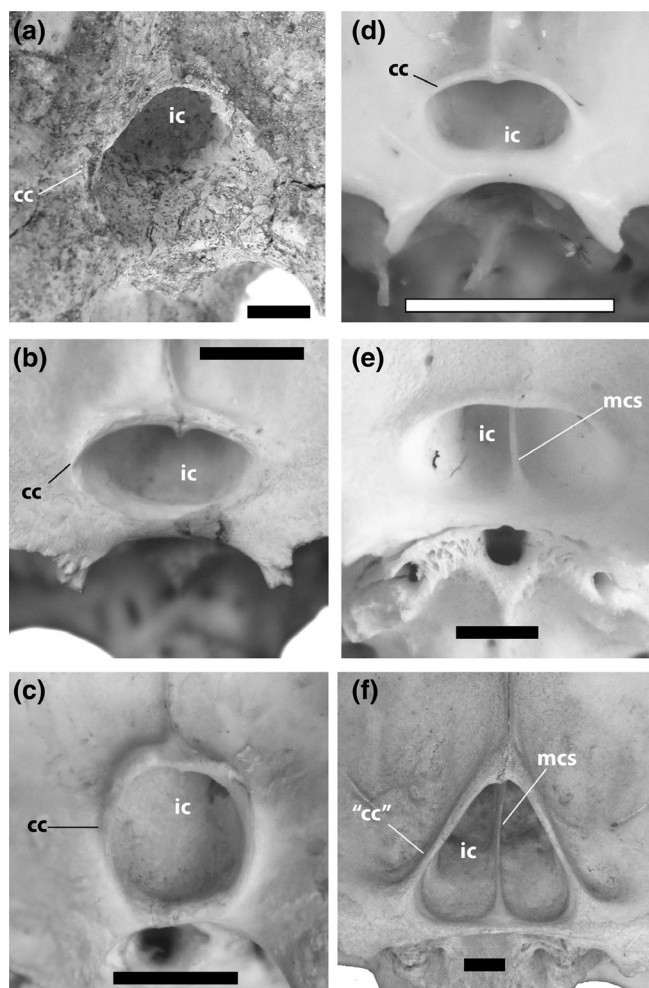
FIGURE 10 Choanae and surrounding area in crocodylids. (a) KNM-MB 29176, holotype, *Kinyang mabokoensis*. (b) FMNH 98936, *Osteolaemus tetraspis* (skull length = 8.2 cm). (c) AMNH R 10083 (holotype), *Osteolaemus osborni*. (d) FMNH 44410, *Osteolaemus tetraspis* (small individual; skull length = 6.2 cm). (e) SUI unnumbered, *Crocodylus niloticus* (small individual; skull length = 18.7 cm). (f) KNM OR 408, *Crocodylus niloticus* (larger individual; skull length = 42.7 cm). Scale = 1 cm (column width)

2.3.2 | Referred material

KNM-KA 68749, large partial skull, jaws, and skeleton (Figures 12 and 13); KNM-KA 66212, incomplete right maxilla (immature; Figure 14); NHMUK PV R 37628, posterior end of right maxilla; NHMUK PV R 37626, partial right surangular; NHMUK PV R 37627, osteoderm (Figure 15). The three specimens from the NHMUK collections may be associated.

2.3.3 | Occurrence

Holotype: Lower Miocene Lokone Member, Lokone Formation, Loperot, southwest of Lake Turkana, Kenya

(Figure 2). Within the Loperot locality, the specimen is from LpM4. Radiometric dates put the age of LpM4 earlier than 17 Ma (Liutkus-Pierce et al., 2019), and faunal analysis indicates strong similarities with the Hiwegi Formation at Rusinga Island, which is approximately 18 Ma in age. Referred Material: Lower Miocene Ngira site, Gully 13, Karungu, near Lake Victoria, Kenya. They were derived from units 21–22 of Driese et al. (2016). Overlying unit 25 has been dated to between 17.7 ± 0.06 and 17.5 ± 0.2 Ma (Drake et al., 1988), dating this material to before 17 Ma, though these dates may have to be revised because of post-depositional alteration (see McCollum et al., 2013; Peppe et al., 2017). A lower Miocene age is nonetheless strongly supported by extensive faunal similarities to the Hiwegi Formation at Rusinga (Driese et al., 2016).

2.3.4 | Etymology

tchernovi, in honor of Dr. Eitan Tchernov, whose work on the crocodile record of North and East Africa in general, and of Kenya in particular, is foundational to current efforts to understand their surprisingly complex regional history.

2.3.5 | Diagnosis

Suborbital fenestra narrow (length-width ratio ≥ 2.27 in morphologically mature individuals). Narial aperture opens anterodorsally anteriorly, but dorsally posteriorly. Maxillary ramus of ectopterygoid convex. Prominent shelves, forming a V-shaped crest, on posterolateral surface of lower jaw (diagnostic for species only if specimens from Karungu and Loperot are conspecific).

2.3.6 | Description

The holotype from Loperot (Figure 11) is a largely complete skull. The pterygoid wings, braincase, right quadrate ramus, and parts of the dorsal rostral surface are not preserved, and the specimen is dorsoventrally compressed, but sutures are clearly visible where bone is preserved. KNM-KA 68749, from Karungu, from a much larger individual, includes the anterior end of the skull fixed to the lower jaw (Figure 12) and associated material (Figure 13). Cranial sutures are much more difficult to trace on the specimen. KNM-KA 66212 (Figure 14) is a partial right maxilla; although substantially smaller than other specimens from Karungu or Loperot, we refer it to *Kinyang* because of the markedly vaulted palate. NHMUK PV R 37628, PV R 37626, and PV R 37627 are
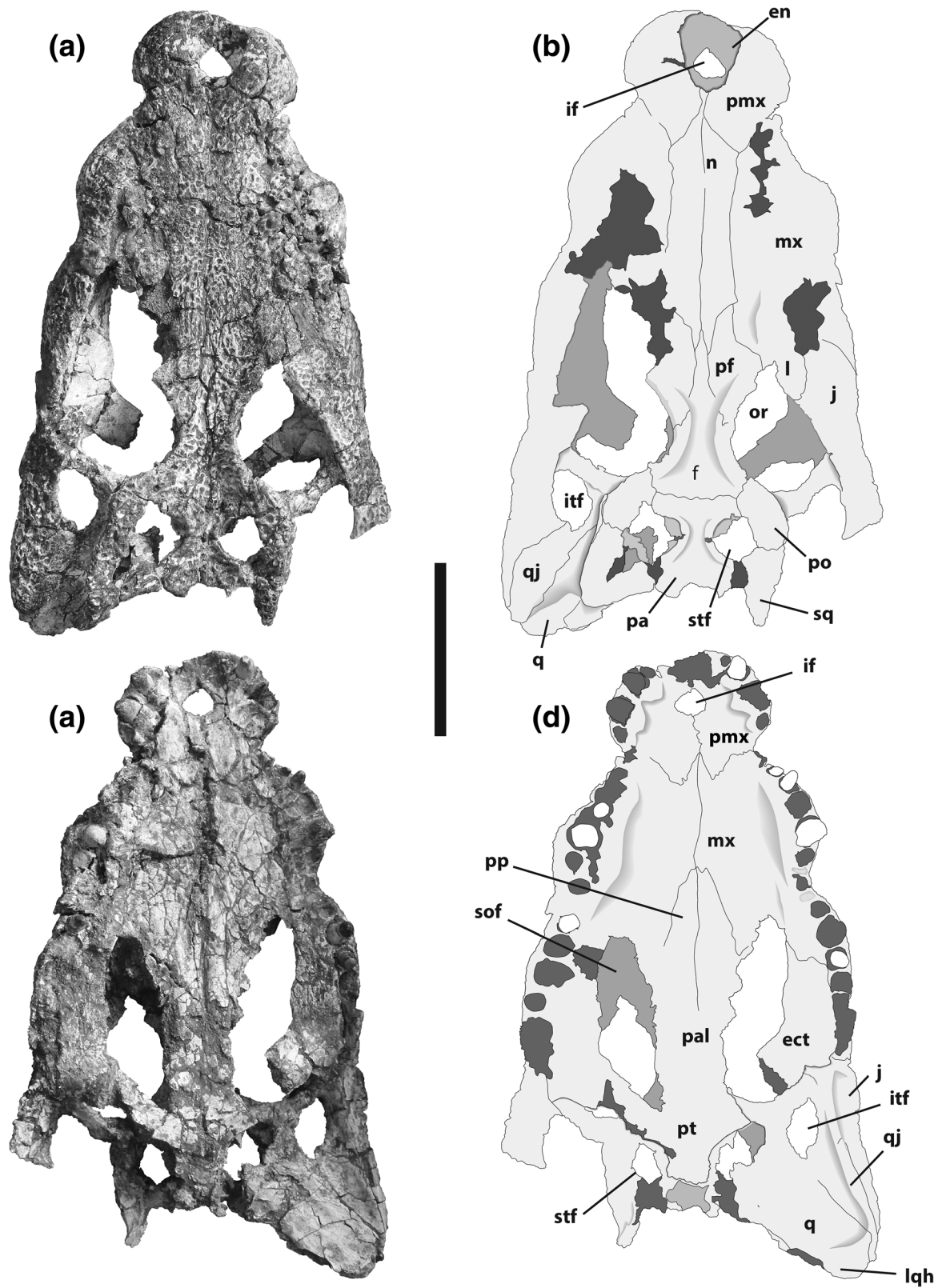
FIGURE 11   KNM-LP 69374, holotype, *Kinyang tchernovi*, Loperot locality. Skull, dorsal (a,b) and ventral (c,d) view. Scale = 10 cm (page width)

referred to *K. tchernovi* based on the broad ectopterygoid shelf evident on a fragment of the right maxilla. Although association of this material cannot be unequivocally demonstrated, its size and overall robustness, along with the absence of duplicated parts, are consistent with a single individual.

FIGURE 12   KNM-KA 68749, *Kinyang tchernovi*, Karungu locality. Partial skull and jaws in dorsal (a) and ventral (b) view. Posteroventral fragment of braincase with occipital condyle, right lateral (c) and posterior (d) view. Partial right articular, dorsal view (e). Fragment of right surangular, lateral view (f). Fragment of right squamosal, dorsal view (g). Scale = 10 cm (a,b) or 5 cm (c–g) (page width)

Each premaxilla bears five alveoli. The second is primarily visible on the right premaxilla, and the fourth is largest. There are deep occlusal pits between the first two alveoli and the third and fourth alveoli. The premaxillary-maxillary suture was W-shaped. The incisive foramen is relatively large and set posterior to the

FIGURE 13 KNM-KA 68749, *Kinyang tchernovi*, Karungu locality. Postcranial material associated with skull and jaws in Figure 11. (a) Axis, right lateral view. (b) Cervical vertebral centrum, left lateral view. (c) Dorsal vertebra from posterior part of series, right lateral view. (d) Base of right scapula, lateral view. (e) Right coracoid, lateral view. (f) Right humerus, ventral view. (g) Proximal end of right radius, lateral view. (h) Distal end of right radius, lateral view. (i) Distal end of right ulna, medial view. (j) Distal end of right ulna, lateral view. (k) Proximal end of right tibia, anterior view. (l) Proximal end of right tibia, posterior view. (m) Osteoderm. Scale = 5 cm (page width)

tooth row. The premaxillae form nearly all of the narial rim, and there is essentially no prenarial rostrum. The lateral margin of the posterior premaxillary process is angled medially and reaches the level of the second or third maxillary alveolus.

The external naris of KNM-LP 69374 is remarkable. As with *K. mabokoensis*, it is comparatively large, and as with *K. mabokoensis*, it opens dorsally along its posterior margin. The premaxillae are inflated in this area. But the narial rim visibly slopes ventrally toward its anterior margin, and the naris thus opens anterodorsally anteriorly (Figure 16). The appearance of this feature is accentuated by damage to the front of the premaxillae, but most of

the narial rim is preserved, and this is not the result of postmortem compression.

The naris of KNM-KA 68749 opens anterodorsally, but not to the same degree as in KNM-LP 69374. There appears to be less disparity in dorsoventral depth between the anterior and posterior margins. However, there is a distinct indentation in the narial rim near the anterior end. This depresses the anteriormost part of the naris. This, too, has been affected by postmortem damage, but surface bone is preserved within the indentation.

The nasals of KNM-LP 69374 can be seen contacting the external naris as a pair of very thin processes between the premaxillae. The same is true, though less clearly, on
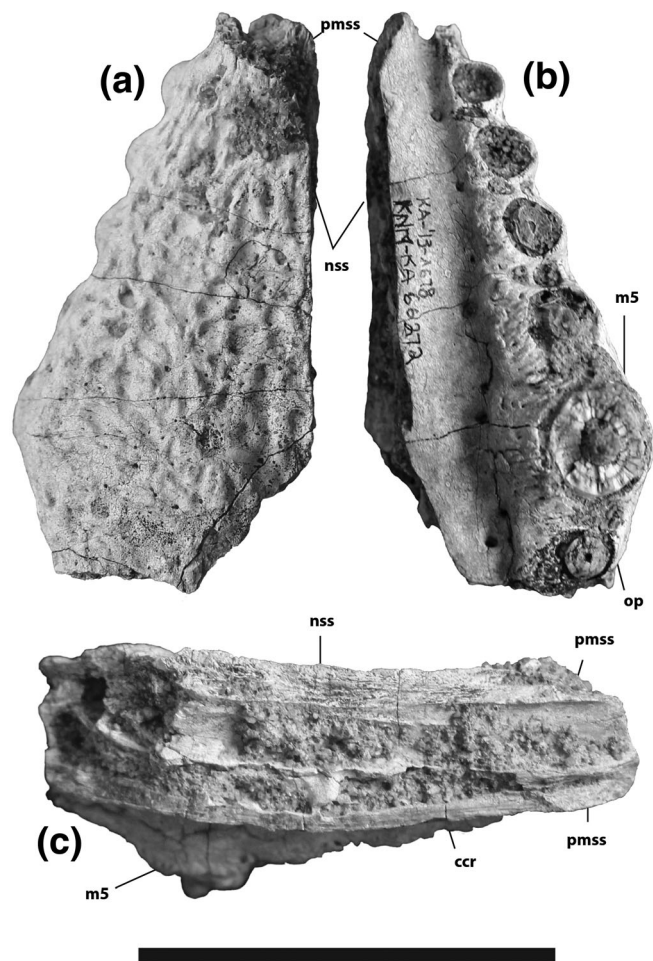
FIGURE 14 KNM-KA 66272, *Kinyang tchernovi*, Karungu locality, partial left maxilla, dorsal (a), ventral (b), and medial (c) view. Scale = 5 cm (column width)

FIGURE 15 *Kinyang tchernovi*, incomplete remains from Karungu. NHMUK PV R 37626, partial right surangular in lateral (a) and medial (b) view. NHMUK PV R 37628, fragment of right maxilla preserving distalmost four alveoli in lateral (c) and ventral (d) view. (e) NHMUK PV R 37627, osteoderm from dorsal shield. Scale = 5 cm (column width)

KNM-KA 68749. Although KNM-LP 69374 is compressed, we do not believe the external exposure of the nasals at the naris is artefactual. The nasals also penetrate the narial chamber ventral to the narial rim on KNM-KA 68749. The lateral margins of the nasals are parallel between the premaxillae and lacrimals, though they are also modestly concave, imparting a constricted appearance to the bones. The nasals taper medially as they pass along the lacrimals and prefrontals, extending between the prefrontals and frontal as a pair of acute processes nearly reaching the level of the orbit.

In dorsal view, the maxillary-premaxillary suture emerges from the occlusal notch for the fourth dentary tooth and extends to the level of m2 or m3. There may have been bosses for the fifth maxillary tooth roots on the holotype, but damage to both elements makes such an assessment difficult. Such bosses are barely present on KNM-KA 68749. Although the anteriormost tip of the right lacrimal can be seen, we do not know whether the maxilla extended posteriorly into the lacrimal.

FIGURE 16 KNM-LP 69374, holotype, *Kinyang tchernovi*, anterior end of rostrum, dorsolateral view. Scale = 2 cm (column width)

Ventrally, the maxillary-premaxillary suture is convex, imparting a W-shape to the suture on an intact skull. The palate adjacent to the first five alveoli is elevated. The maxillae contact the palatines posteromedially and

extend between the palatines and suborbital fenestrae for a short distance.

A precise maxillary tooth count is difficult to assess. The tooth row is largely obscured on KNM-KA 68749. Although exposed on the holotype, the distalmost alveoli are poorly preserved. The right 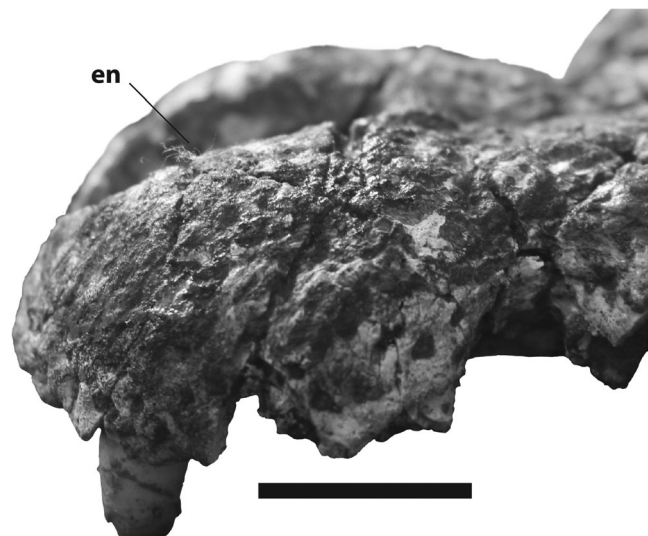maxilla shows clear evidence for 12 alveoli, but there is sufficient room between m12 and the jugal for an additional alveolus. Preservation is worse on the left maxilla, but again, the space available where the tooth row would have been is consistent with 13 alveoli.

The lacrimal outlines are not well preserved, but they extended further anteriorly than the prefrontals. The right lacrimal of the holotype preserves a modest longitudinal crest. The prefrontals are crescentic, terminating anterior to the frontal anterior process. The remnants of prefrontal pillars are visible on the holotype, but nothing meaningful can be said beyond their presence.

The frontal bears a slender, acute anterior process that passes between the nasals. The frontal-prefrontal suture intersects the orbit at a high angle, but not perpendicular to it. The dorsal surface of the frontal is concave and the orbital rim is thus upturned. Although there is damage to the frontal posteriorly, the frontoparietal suture was entirely on the skull table surface and linear. There is a sagittal groove on the ventral surface of the frontal for the olfactory tract.

The postorbital bears a crescentic dorsal body forming the posterior margin of the orbit and anterolateral margin of the supratemporal fenestra. The slender, columnar descending ramus, inset ventral to the dorsal body, forms the dorsal part of the postorbital bar.

Because the lateral surfaces of the squamosals are oriented anteromedially, the skull table is somewhat trapezoidal in shape. Although the dorsal surfaces are damaged, there is no indication of an upturned squamosal boss. The lateral groove for the ear flap musculature has parallel dorsal and ventral margins. The squamosal-postorbital suture extends anteriorly ventral to the groove to the postorbital bar. The degree to which the squamosal forms the margin of the otic aperture is unclear. The squamosal extends posterolaterally along the paroccipital process.

The parietal lies between the circular supratemporal fenestrae. Its sutural contact with the frontal is linear and entirely on the dorsal surface of the skull table. The parietal extended to the posterior margin of the skull table, but because this surface is damaged at the midline, we cannot tell if it was disrupted by a dorsal exposure of the supraoccipital.

The anterior margins of the jugals are not well preserved, but their lateral surfaces anteriorly, lateral to the orbits, are flattened. An ascending process forms the ventral part of each ventrally inset postorbital bar, but the contact between the jugal and postorbital cannot be seen. The jugal is mediolaterally compressed ventral to the infratemporal fenestra, with a convexity on its ventrolateral surface bearing a ventral fossa, and the jugal forms the posteroventral corner of the fenestra. The medial surface is damaged on the left and covered with matrix on the right, preventing us from determining the size of the jugal foramen.

Anteriorly, the quadratojugal extends from the dorsal angle of the infratemporal fenestra. Because the posterior margin of the fenestra is damaged, we cannot tell if the quadratojugal bore an anterior spine. The quadratojugal expands posterior to the infratemporal fenestra and extends almost to the posterior end of the quadrate ramus.

The quadrate forms most of the surface of the otic recess ventral to the skull table. A curved discontinuity emerging from the posterior margin of the left otic aperture may be the squamosal-quadrate suture, but it could also be a crack. A fragment of the right quadrate, however, is less ambiguous—the suture itself is not preserved, but the quadrate can clearly be seen forming the posterior wall of the otic aperture, at least ventrally. There is no indication of a preotic foramen, but again, this area is damaged. The left quadrate ramus is incomplete medially, and neither the medial hemicondyle nor quadrate foramen aëreum are preserved. Bosses on the ventral surface for the adductor musculature are not prominent.

The conjoined palatines bear an anterior process extending to the level of m7. The anterior end of the process is broad and almost linear, and the lateral margins are oriented anteromedially. The palatines form the medial borders of the suborbital fenestrae, and they are flared anteriorly. The suture with the pterygoids is linear and located forward of the posterior margins of the fenestrae.

The maxillary ramus of the ectopterygoid is robust, with a broad, flattened ventral surface that projects laterally, forming a concavity in the outline of the suborbital fenestra. Based on the left ectopterygoid, the maxillary ramus extended anteriorly to the level of m9, forming a slender, acute process and abruptly expanding laterally adjacent to m10. Although not forked in the strictest sense, the anterior end is nevertheless deeply cleft. The ascending rami formed part of the postorbital bar, but to an unknown degree.

The pterygoids appear to have been concave anterior to the choana, but the choana itself is not preserved. Neither are the pterygoid wings.

Very little can be said of the occipital surface or braincase. The supraoccipital is too damaged to assess. The skull table appears to have extended posteriorly dorsal to

the occipital surface. The paroccipital process of the left exoccipital is preserved in contact with its corresponding squamosal. The basioccipital bears a rounded occipital condyle, but although the exoccipital appears not to have extended ventrally to the basioccipital tubera, this cannot actually be determined, because the tubera themselves are not preserved. Likewise, the right lateral carotid foramen and vagus fossa are visible, and the carotid foramen was dorsal to the D-shaped posterolateral exposure of the basisphenoid.

The lower jaw is not known from Loperot. The skull and jaws are in occlusion in KNM-KA 68749, preventing us from seeing many details (including the dentary tooth count), but we can nonetheless make some observations about the lateral and medial surfaces. The dentary symphysis extends to approximately the level of d5 or d6 based on its length, but we cannot rule out slightly shorter (d4) or slightly longer (d7) symphyses. The imperforate splenials do not meet at the midline, and the anterior tip of the splenial is slightly longer ventral to the Meckelian groove than dorsal to it. The external mandibular fenestra is similar and shape and size to that of *K. mabokoensis*, but sutural details are difficult to see. The collateral ligament pit was subdivided. The surangular did not extend to the dorsal tip of the posterior glenoid fossa wall.

There are robust shelves on the lateral surface of the right mandibular ramus immediately anterior to the articular. A lateral shelf along the dorsal margin of the surangular is seen in several short-snouted crocodyliforms (see below), but this specimen also bears a similar that extends from the posterior end of the dorsal shelf along the posteroventral margin of the lateral sculpted surface. These meet posteriorly to form a prominent V-shaped crest, with its apex lateral to the glenoid fossa. Although what is known of the left ramus is insufficient to assess the presence of the ventral shelf, a fragment of the left surangular includes the dorsal shelf, suggesting the feature was at least symmetrically present on the specimen and not pathological in origin.

Part of the left hyoid is preserved fixed to the pterygoid. The anterior projection is a flattened structure, but the dorsal projection is not preserved.

KNM-KA 68749 includes postcranial material. It is consistent with an animal of the same size as the skull, and there are no duplicated elements. Moreover, the skull and postcranial remains were collected in the same wash. We therefore accept the association. The vertebrae are strongly procoelous, and their neurocentral sutures are either completely or partially closed, with partially closed sutures prevailing in the cervical region. A single cervical centrum preserves sutural surfaces for the neural arch peduncles; this might at first suggest open sutures,

but specimens with partially closed sutures maintain cartilaginous laminae between the neural arch and centrum (i.e., they are not actually fused), and no other cervical shows open sutures. It is simplest to assume the specimen with sutural surfaces broke along partially closed but still weak sutural contacts.

The atlas-axis complex is represented by the atlas intercentrum, poorly preserved atlas neural arches, and nearly complete axis. The atlas intercentrum is wedge-shaped in lateral view and although the parapophyseal surfaces are prominent, the parapophyses themselves are not broadly separated. The axial centrum bears a sagittal hypapophysis at its anterior end, immediately behind the odontoid. The neural spine is incomplete, but its dorsal surface is horizontal anteriorly and oriented posterodorsally as it approaches the level of the postzygapophyses. There is no trace of either the axial neurocentral suture or the suture between the axial centrum and odontoid.

There are several pectoral elements associated with the specimen. Neither the scapular nor coracoid blades are preserved, but their bases indicate a comparatively broad articulation surface adjacent to the shoulder socket. The deltoid crest of the scapula was broad and set in somewhat from the anterior surface of the bone. The only completely preserved appendicular bone is the right humerus, which is morphologically consistent with most crocodylian humeri—its deltopectoral crest is concave proximally, there is only a single insertion tubercle for the teres major and dorsalis scapulae musculature, and the bone as a whole bears proportions similar to those of extant crocodylian humeri from animals of similar size. The proximal end of the ulna has a broadly rounded olecranon.

Osteoderm morphology varies, presumably based on location on the body. Several subrectangular osteoderms with smooth anterior imbrication zones are from the dorsal shield. All bear keels.

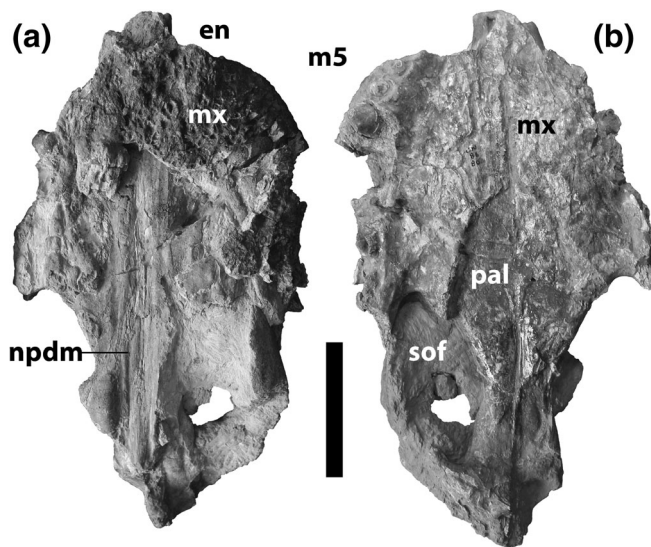## 2.4 | *Kinyang* sp. (Chianda locality)

2.4.1 | Referred material

KNM-CU 10511 (Figure 17), incomplete skull with central region of palate, small amount of dorsal rostrum surface, and natural molds of the nasopharyngeal duct and rostral pneumatic structures.

2.4.2 | Occurrence

Chianda, Uyoma Peninsula (Figure 2). The fauna recovered from the Uyoma Peninsula is equivalent to that of

FIGURE 17 KNM-CU 10511, *Kinyang* sp., Chianda locality, partial skull in dorsal (a) and ventral (b) view. Scale = 10 cm (column width)

FIGURE 18 KNM-MO 90, *Kinyang* sp., Moruorot locality. Right quadrate ramus, dorsal (a) and ventral (b) view. Left quadrate ramus, dorsal view (c). Fragment of left maxilla and ectopterygoid, ventral (d) and lateral (e) view. Incomplete right surangular and angular, lateral view (f). Scale = 5 cm (column width)
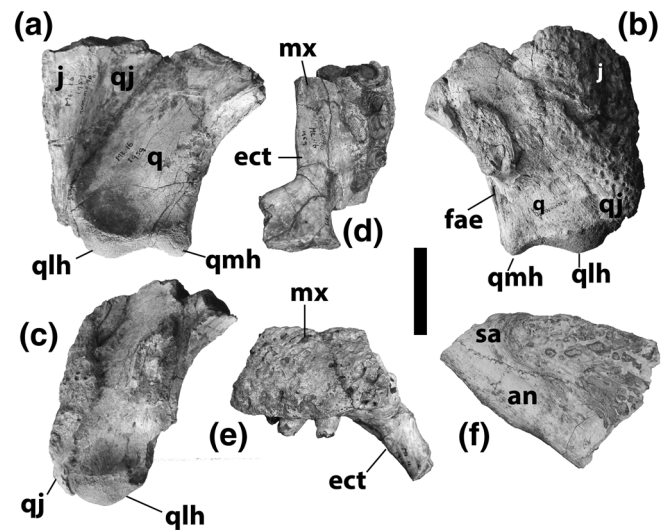
Rusinga, which is conservatively dated to between 17 Ma and 20 Ma (Peppe et al., 2017; Pickford, 1986).

2.4.3 | Discussion

The only specimen from Chianda that can be referred to *Kinyang*, KNM-CU 10511, is an incomplete skull. Very little of the dorsal surface of the rostrum is preserved. The concavity at the front of the specimen is the posterior wall of the narial chamber, but sutures cannot be traced. But several aspects of the internal morphology of the rostrum are preserved as natural molds. Parallel cylindrical structures represent the nasopharyngeal duct. An irregular expansion of the matrix where the dorsal surface of the left maxilla has worn away is here interpreted as a mold of the caviconchal recess, and a rounded protuberance dorsolateral to the left palatine may indicate a pterygoid bulla.

The maxilla is highly vaulted medial to the first five alveoli. The palatine process is U-shaped, but the lateral margins are oriented anteromedially and not parallel with each other. The former is consistent with *Kinyang*, and the latter is diagnostic for it.

The suborbital fenestra appears to have been comparatively wide. Maximum width cannot be measured, but its overall shape is more similar to that of *K. mabokoensis* than that of *K. tchernovi*. However, the specimen is too incomplete to comfortably refer to any particular species.

2.5 | *Kinyang* sp. (Moruorot locality)

2.5.1 | Referred material

KNM-MO 90 (Figure 18), fragments of skull and lower jaw including both quadrate rami; part of the left maxilla, ectopterygoid, and jugal; the articular region of the right mandibular ramus; and additional craniomandibular pieces.

2.5.2 | Occurrence

Kalodirr Member, Lothidok Formation, Moruorot, west of Lake Turkana (Figure 2). Radiometric dates from under- and overlying tuffs bracket the age of these deposits to between 17.7 and 16.6 Ma (Boschetto et al., 1992).

2.5.3 | Discussion

This specimen is represented by chunks of skull and lower jaw, most of which hold little systematic value, but three features merit discussion. The first is the left ectopterygoid; little remains of the pterygoid ramus, but the maxillary ramus is preserved in articulation with the maxilla. The anterior end is deeply cleft, but the maxillary ramus of this specimen is also mediolaterally broad.

As a result, the margin between the two anterior projections is almost linear. It forms the medial margin of the distalmost two alveoli, and extends forward medial to two additional alveoli. A fragment of the left maxilla and squamosal suggests a similar condition, but only one dorsal projection—the one that would be visible on the palatal surface—is preserved.

The second and third important features are preserved on the right surangular, which is preserved in articulation with the articular and angular. The dorsal fossa for the lateral collateral ligament is subdivided, and although the posterior surface of the glenoid fossa is damaged, the dorsal surangular lamina lateral to it is low and flattened, indicating the truncated condition. The lateral surface lacks the prominent shelves seen in *K. tchernovi* from Karungu. Assuming the shelves are a consistent feature in *K. tchernovi*, we can reject referral to that species; nevertheless, the truncated dorsal surangular lamina is found in both *K. tchernovi* and *K. mabokoensis*, and *K. mabokoensis* also has a subdivided collateral ligament pit on the surangular. These features support referral to *Kinyang*.

3 | MATERIALS AND METHODS

3.1 | Parsimony analysis

We conducted maximum parsimony analyses based on a matrix of 195 discrete morphological characters and 47 ingroup taxa (Data S1). The matrix is based on that of Brochu and Storrs (2012), but with characters added to express variation among crocodylids. Trees were rooted using *Borealosuchus sternbergii* (Gilmore, 1910) as an outgroup. Notably, 1,000 random-seed heuristic searches were conducted in PAUP* 4.0a169 (Swofford, 2002). Multistate characters were left unordered, and all characters received equal weight.

Six new characters were added to the matrix:

190: Maxilla-premaxilla suture on palate W-shaped (0) or U- or V-shaped (1). This refers to the suture with the left and right maxillae and premaxillae in articulation. The sutures on either side of the sagittal plane converge anteriorly in some forms, but posteriorly in others. Among crocodylids, W-shaped sutures are seen in *Mecistops*, most species of *Crocodylus*, *Kinyang*, and *"Crocodylus" gariepensis*. U- or V-shaped sutures occur in *Osteolaemus*, *Voay*, *Euthecodon*, and *Brochuchus*. The acuteness of the midpoint of the suture varies within species, which is why we did not treat U-shaped and V-shaped sutures as different states.

The suture in the specimen of *Rimasuchus lloydi* used in this and all previous phylogenetic analyses (NHM PV R14154), which comes from the type locality in Egypt, appears to us to be U-shaped, but sutures on that part of the skull are imperfectly preserved enough to leave open the possibility of the opposite state. Moreover, specimens referred to *R. lloydi* from slightly younger deposits in Libya (Llinas Agrasar, 2004) bear W-shaped sutures, albeit with a short midline process of the conjoined maxillae resembling that of *"C." gariepensis*. A short process such as this could be easily masked by postmortem distortion.

191: Frontal terminates posterior to anteriormost extent of prefrontal (0) or frontal and prefrontals terminate nearly in the same transverse plane (1). The prefrontals extend further anteriorly than the frontal in most crocodylians. This is not the case in *Mecistops*, in which the prefrontals and frontal extend to approximately the same transverse plane. This is because the prefrontals are short, not because the frontal is long.

192: Nasals separate (0) or fused (1) at maturity. It can often be difficult to find the suture between the nasals in fossil skulls. This is nearly always a matter of preservation—the suture simply cannot be seen. The nasals of *Euthecodon*, however, are unambiguously fused. No trace of a suture has been found in any of the many *Euthecodon* specimens we have examined, many of which preserve other sutures clearly. Skulls from very young specimens of *Euthecodon* have not been identified, and so we do not know whether this condition pertained throughout posthatching ontogeny.

193: Minimal prenarial rostrum (0) or substantial prenarial rostrum (1). In modern species of *Crocodylus*, the premaxillae extend anterior to the naris to a greater extent than in other crocodylians (Figure 5b), including Paleoafrican *Crocodylus* (Brochu et al., 2010: Figure 1). The only fossil species in our data set sharing this feature is Turkana *C. checchiai*, though we might reconsider this decision as we re-evaluate *C. checchiai* from Libya. In other crocodylids, including *Kinyang* (Figure 5a), the naris lies much closer to the anterior tip of the snout.

One would think that the slender-snouted forms in our data set would also have the derived condition. But in fact, only the alveoli for d1 are elongated in these forms. The prenarial rostrum in *Crocodylus* includes d2 and d3.

194: Maxilla bears 12 or 13 (0), 13 or 14 (1), 14 to 16 (2), 17 to 19 (3), 20 to 22 (4), 23 to 24 (5), or more than 24 (6) teeth. Characters similar to this have appeared in other phylogenetic analyses (e.g., Jouve, 2007; Lee & Yates, 2018; Rio & Mannion, 2021). That the character states overlap is discussed below.

195: Pit for lateral collateral ligament on surangular single (0) or subdivided (1). Subdivided pits are only found in *Kinyang* (e.g., Figure 7g,h).

3.2 | Bayesian inference analysis

We also conducted an analysis using Bayesian inference on data sets that combined molecular and morphological information. We used the mtDNA data analyzed by Hekkala et al. (2021), which includes DNA extracted from subfossil remains of extinct *Voay robustus* from Madagascar. The morphological data set used by Hekkala et al. (2021), which was derived from that of Lee and Yates (2018), was replaced with ours. We used their alignments and we excluded from our analyses the sequences from taxa that are not included within our morphological dataset (e.g., Alligatoridae, *Gavialis*, some of the outgroup taxa).

The best nucleotide substitution models for each of the 15 mitochondrial genes from the Hekkala et al. (2021) data set were selected using JModelTest v.2.1.10 (Darriba et al., 2012; Posada, 2008), according to the Akaike Information Criterion for small sample sizes (AICc; Akaike, 1973). The DNA sequences were manually concatenated with the morphological data, resulting in a dataset with 14,174 DNA base pairs and 195 discrete morphological characters from 51 taxa (Data S2). The Markov k model of character evolution (Mk model; Lewis, 2001) was implemented in the morphological data partition and *Borealosuchus sternbergii* was established as the outgroup. Phylogenetic reconstructions were obtained through Bayesian inference carried out with MrBayes v.3.2.7a (Huelsenbeck & Ronquist, 2001; Ronquist & Huelsenbeck, 2003) at the Centro de Computación de Alto Rendimiento CCAR-UNED. The analysis was run for 50 million generations with 2 simultaneous runs. A 25% burn-in was implemented after assessing stationarity and convergence of continuous parameters with Tracer v.1.7.2 (Rambaut et al., 2018). The Effective Sample Size (ESS) value was above 200 and the Potential Scale Reduction Factor (PSRF) value was 1.

3.3 | Taxon sampling

Kinyang tchernovi is based on data from both Loperot and Karungu. Experiments with codings modified to exclude Karungu material do not change the resulting tree topologies.

We include both living species of *Mecistops* Gray, 1844—*M. cataphractus* (Cuvier, 1825) and *M. leptorhynchus* (Bennett, 1835). The only morphological character separating them in our matrix concerns the presence of upturned squamosals in *M. cataphractus*. The squamosal horns of *M. cataphractus*, described as "nubbins" by Shirley et al. (2014), are not nearly as prominent

as in other forms sharing this state, such as *Voay* and Paleoafrican *Crocodylus*, but the condition between the two species is sufficiently different to justify assigning different states. We also include both species of Neoafrican *Crocodylus*; although their morphological expressions in this matrix are the same, molecular data clearly differentiate them.

Although we include specimens from the Late Miocene at Lothagam referred to *Crocodylus checchiai* by Brochu and Storrs (2012), we do not include material from the type locality in Libya. The Libyan material was recently reviewed by Delfino et al. (2020), whose results suggested a distant relationship between the Libyan and Kenyan forms and a close relationship between Libyan *C. checchiai* and Neotropical *Crocodylus*. Following recent first-hand assessment of some of the Libyan material by one of us (CAB), we interpret some aspects of its morphology differently. A full discussion is beyond the scope of this article.

Asiatosuchus nanlingensis Young, 1964 from the Middle Eocene of China is included in this analysis. Codings are based on direct study of the material, which includes specimens formerly referred to *Eoalligator chunyii* Young, 1964 from the same deposits. Based on our observations, we concur with Wang et al. (2016) and consider *E. chunyii* to be a junior synonym of *A. nanlingensis*. We disagree with the arguments presented by Wu et al. (2018) in support of their species-level separation.

Codings for *Asiatosuchus grangeri* Mook, 1940 have been revised following a reconsideration of the morphology of referred material. Codings for *Crocodylus anthropophagus* Brochu et al., 2010 have been modified following Azzarà et al. (2021).

Sampling among taxa falling out as tomistomines in most morphological analyses was reduced, and *Gavialis* was left out entirely. This was intended to streamline the analysis by limiting points of disagreement between different analyses that are not central to the relationships of *Kinyang*. No analysis published to date using a version of this matrix has found support for a close relationship between any of the crocodylids analyzed here and anything that might be regarded as a gharial.
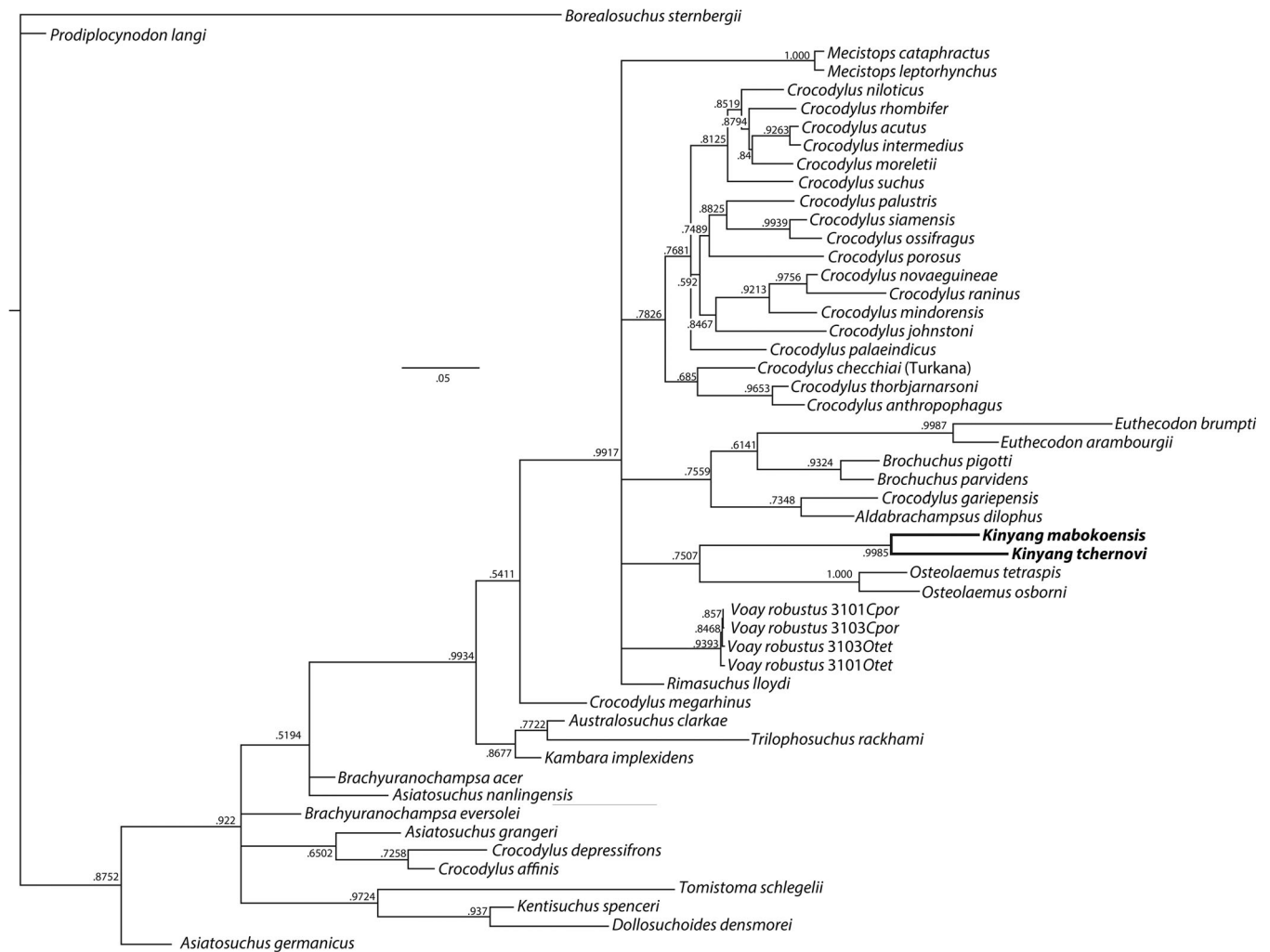
4 | RESULTS

4.1 | Parsimony analysis

The maximum parsimony analysis recovered 12 equally optimal trees (length = 278, CI without uninformative characters = 0.463, RI = 0.713). The consensus trees derived from these results (Figure 19) are largely congruent with those of previous analyses based on this matrix
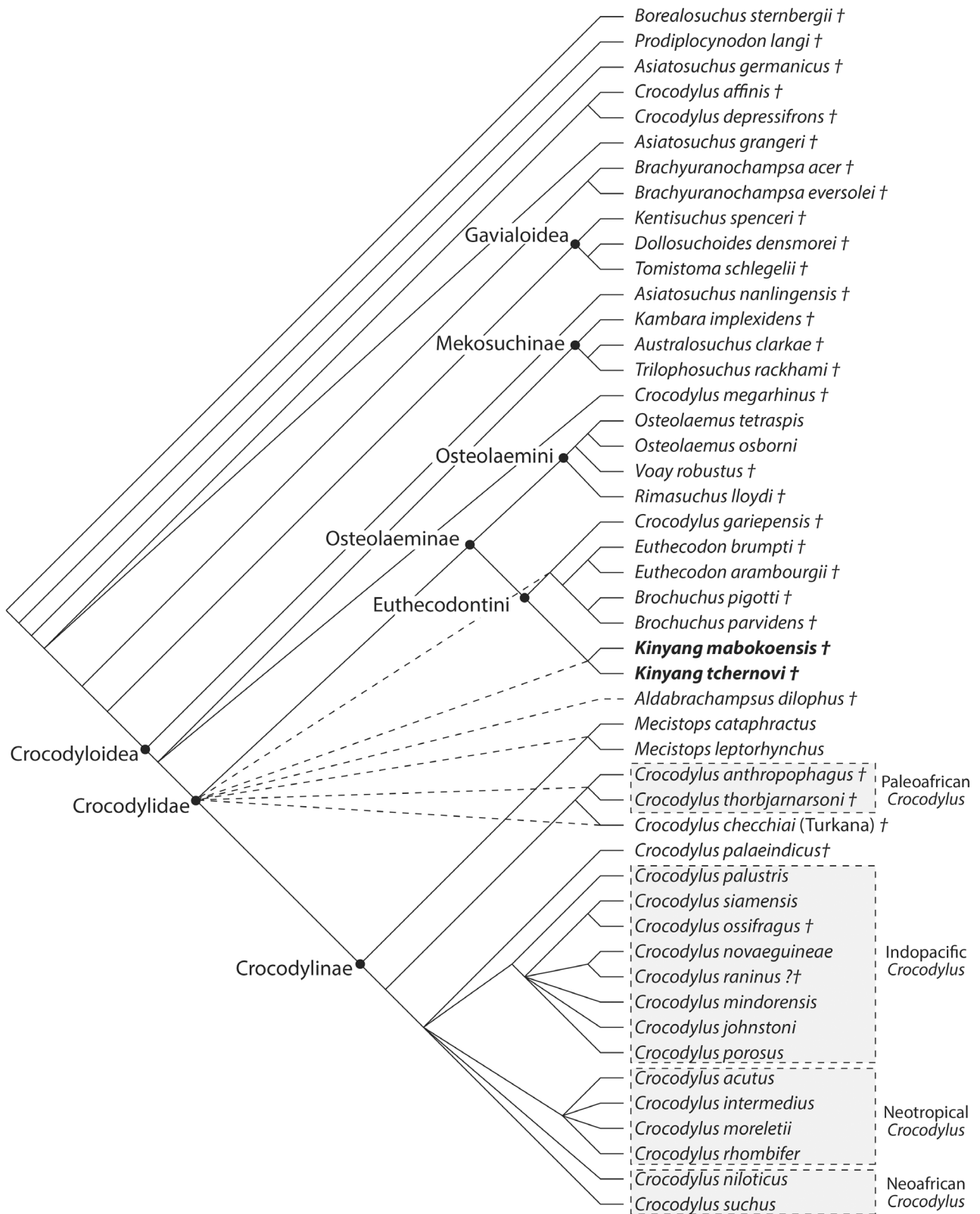
FIGURE 19 Results of maximum parsimony analysis of 194 morphological characters. Solid lines indicate relationships in Adams consensus of 12 equally optimal trees if *Aldabrachampsus dilophus* is included (length = 278, CI = 0.463) and strict consensus of 6 equally optimal trees if *A. dilophus* is excluded (length = 277, CI = 0.465). Dotted lines indicate lost resolution in a strict consensus tree with *A. dilophus* included (page width). † is a standard indicator for extinct taxa

FIGURE 20 Majority-rule consensus tree showing results of Bayesian analysis of mtDNA from Hekkala et al. (2021) and 195 morphological characters. Numbers at nodes represent posterior probabilities (page width)

(e.g., Brochu & Storrs, 2012; Cossette et al., 2020), but resolution among crocodylids in the strict consensus is low. An Adams consensus recovers some of the topology lost by the inclusion of incompletely-known, and thus labile, *Aldabrachampsus dilophus* Brochu, 2006. Exclusion of *A. dilophus* results in six equally optimal trees (length = 277, CI without uninformative characters = 0.465, RI = 0.713) with a strict consensus (Figure 20) topologically matching that of the Adams consensus of the full set of taxa.

Several aspects of these results are worth mention. First, with *Aldabrachampsus* excluded, Paleoafrican *Crocodylus* and Turkana *C. checchiai* form a clade outside crown-genus *Crocodylus*. In several previous analyses, Paleoafrican *Crocodylus* and Turkana *C. checchiai* independently were part of a polytomy including *C. palaeindicus* as well as Neoafrican, Neotropical, and Indopacific *Crocodylus*. In this, our results replicate those of Azzarà et al. (2021), who also recovered a monophyletic Paleoafrican assemblage exclusive of extant *Crocodylus*, though that analysis did not include Turkana *C. checchiai*.

Second, these results objectively exclude *Aldabrachampsus* from *Crocodylus*. A previous analysis including this diminutive form (Brochu, 2006) found that *Aldabrachampsus* assumed one of two positions in the set of optimal trees—either as an osteolaemine or related to *Crocodylus palaeindicus* Falconer, 1859. Here, it falls in one of two places. In one, it is closely related to *Crocodylus thorbjarnarsoni* and *C. anthropogagus*. In the other, it is a euthecodonin osteolaemine related to "*Crocodylus*" *gariepensis*. This bimodal position explains the collapse of Osteolaeminae and the imprecise position of Turkana *C. checchiai* in the strict consensus tree.

Our analysis also suggests that *Asiatosuchus nanlingensis* is more closely related to Crocodylidae than are the gharials. This contrasts with the results in previous analyses, where *A. nanlingensis* assumed a more

basal position among crocodyloids (or stem longirostrines) or (in its incarnation as *Eoalligator chunyii*) as an alligatoroid along with the enigmatic Southeast Asian orientalosuchins (e.g., Wang et al., 2016; Wu et al., 2018; Massonne et al., 2019; Groh et al., 2020; Shan et al., 2021).

Kinyang mabokoensis and *K. tchernovi* are recovered as osteolaemines. Together, they are in a sister group relationship with a clade including *Euthecodon*, *Brochuchus*, and *"Crocodylus" gariepensis* within Euthecodontini.

4.2 | Bayesian inference analysis

The results of the combined mtDNA-morphological analysis (Figure 20) are consistent with those of the parsimony analysis of morphology (Figure 19). They are also largely consistent with those obtained by Hekkala et al. (2021) using the same mtDNA data, though there are some points of phylogenetic disagreement that cannot be dismissed as artifacts of dampened resolution. In particular, *K. mabokoensis* and *K. tchernovi* are more closely related to *Osteolaemus* than to *Crocodylus* in this analysis.

Some differences between our results and those of Hekkala et al. (2021) undoubtedly reflect differences in the morphological data. In particular, Hekkala et al. (2021) recovered a close relationship between *Euthecodon* and *Mecistops*. Hekkala et al. (2021) used the morphological data set of Lee and Yates (2018), who also recovered a *Euthecodon-Mecistops* grouping. Lee and Yates (2018) relied on Conrad et al. (2013) for data on *Brochuchus*, and our scores for *Brochuchus* (as well as other crocodylians) differ in several ways (Cossette et al., 2020). Support for a *Brochuchus-Euthecodon* relationship in our combined analysis was comparatively low (posterior probability value of .6141), but this is nonetheless consistent with the morphology analysis.

The most notable difference between our results and those of Hekkala et al. (2021) reflect resolution. *Crocodylus* is monophyletic, and it includes the familiar Paleoafrican, Indopacific, and Neotropical groups, and consistent with previous molecular analyses (e.g., Hekkala et al., 2011; Meredith et al., 2011), the Neoafrican assemblage is paraphyletic with respect to the Neotropical clade. But our results do not recover a monophyletic Osteolaeminae conforming with anything recovered in our morphological analysis or by Hekkala et al. (2021). We recovered a polytomy including *Mecistops*; *Voay*; *Rimasuchus*; a Euthecodonini comprising *Euthecodon*, *Brochuchus*, *"Crocodylus" gariepensis*, and *Aldabrachampsus*; and a group including *Osteolaemus* and *Kinyang* (Figure 20).

There are several possible explanations for the loss of resolution in our results. The first could be the exclusion of *Gavialis* and the alligatorids in our analysis. Another is the use of different morphological sets; ours might provide stronger support for an osteolaemine affinity for *Voay* than that of Lee and Yates (2018), rendering the analysis incapable of pinpointing its relationships to either *Crocodylus* or *Osteolaemus*. Further analyses are needed to explore these issues.

Notably, our results still support an osteolaemine affinity for *Kinyang*. Indeed, in this analysis, *Kinyang* is the only unambiguous osteolaemine in the sample of taxa, albeit with modest support (posterior probability value of .7507).

5 | DISCUSSION

5.1 | Monophyly of *Kinyang*

These two species are very similar, and evidence for their close relationship is substantial. Both had short, robust snouts, with virtually no prenarial rostrum; inflated premaxillae around the naris (at least posteriorly); and ventrally broad, flattened ectopterygoids adjacent to the maxillary tooth row. The shape of their palatine processes—flattened anteriorly, but with anteriorly-converging lateral margins—is unique among crocodylids.

Four characters provide unambiguous support for the monophyly of *Kinyang* in our analysis. The first is what appears to be a less derived occlusal pattern. In both species, there are occlusal pits between m6 and m8, but nowhere else in the maxillary toothrow. In contrast, occlusal pits occur more extensively between m1 and m6 in all other crocodylids.

Ancestrally, crocodylians have a complete overbite behind the maxillary-premaxillary notch. Interfingering dentition arose independently in multiple crocodylian clades, with an intermediate condition—occlusal pits between m6 through m8, but lingual to the maxillary alveoi proximally—sometimes occurring at phylogenetic levels rootward of those with full interdigitation (Brochu, 2003). The ingroup in this analysis preserves what appears to be a transitional series from full overbite (*Prodiplocynodon langi*, *Asiatosuchus germanicus* Berg, 1966) to full interdigitation (crocodylids, gavialoids, *Brachyuranochampsa* Zangerl, 1944) with a handful of Eocene stem longirostrines (e.g., *"Crocodylus" affinis*) having occlusal pits limited to m6 through m8. Reversals to a partial or complete overbite are uncommon, to our knowledge only having happened among mekosuchines (Buchanan, 2009; Iijima, 2017; Molnar, 1981) in addition to *Kinyang*.

The second unambiguous synapomorphy in this analysis actually has a convoluted history among crocodylids.

In both species of *Kinyang*, the quadratojugal extends anterodorsally to the dorsal corner of the infratemporal fenestra, largely blocking the quadrate from the posterior margin of the fenestra (Figure 6). This is the ancestral condition for Crocodylia, and it pertains to Paleoafrican *Crocodylus*, Turkana *C. checchiai*, and to extant *Osteolaemus* and *Crocodylus novaeguineae* Schmidt 1928, as well as possibly extant *C. raninus* Müller and Schegel, 1844. This character could not be assessed for either species of *Brochuchus*.

The third unambiguously diagnostic character for *Kinyang* in this analysis is the subdivided lateral collateral ligament (Figure 7g,h). This is known in no other crocodylian. The functional or biomechanical reason for this subdivision is unclear, but it clearly differentiates *Kinyang* from all other crocodylids.

The fourth synapomorphy for *Kinyang* is based on the number of maxillary teeth. In *Kinyang*, each maxilla has either 12 or 13 alveoli. This is also true in *Osteolaemus* and *Voay*. In contrast, other crocodylids typically have at least 14. This merits further discussion, both because the typical number in *Kinyang* is unclear and, because tooth counts in extant crocodylians can vary to a modest degree, states used here to express the maxillary tooth count overlap.

Most of the *Kinyang* maxillae described here either preserve an incomplete tooth row or are insufficiently preserved posteriorly to fix the absolute number of tooth positions. One specimen of *K. mabokoensis* (KNM-MB 25757) preserves 12, but other specimens are consistent with 13. Because the specimens themselves are ambiguous, so is our assessment of the maxillary tooth count in *Kinyang*—it is 12 or 13.

Although the maxillary tooth row can vary by one alveolus in crocodylians, variation is always caused by a small number of specimens that appear to have lost an alveolus at some point in life. Variation in crocodylians is always to have a handful of individuals with fewer alveoli, not more. Taxa with state 1 nearly always have 14 alveoli. Individuals of species that otherwise have 14 alveoli, but which have 13, are frequently asymmetrical—one maxilla has 13, and the other 14—and the missing alveolus is typically the last in the series (CAB, personal observation).

We acknowledge the ambiguity the overlapping character states in this analysis can cause. Nevertheless, although we are unsure whether *Kinyang* typically had 12 or 13 maxillary alveoli, we are very confident it did not have 14 or more. We scored both species accordingly. Had only one complete maxilla been known for *Kinyang*, we would have been unable to assign a state to either species.

We propose that the lack of complete interdigitation and the reduced number of maxillary teeth may reflect changes in the size and distribution of maxillary alveoli, which appear to be larger and more closely spaced than in other crocodylids of similar size (personal observation). This would have been inconsistent with the presence of occlusal pits between most alveoli, and there may no longer have been sufficient space for the additional alveoli seen in other crocodylids. In this sense, *Kinyang* is the opposite of *Brochuchus*, in which maxillary alveoli and teeth are comparatively small and widely spaced (Conrad et al., 2013; Cossette et al., 2020).

5.2 | Differentiation of *Kinyang mabokoensis* and *Kinyang tchernovi*

Differences between the two species are subtle, but consistent. For example, the suborbital fenestra is comparatively wider in *K. mabokoensis* than in *K. tchernovi*. In both skulls referred to *K. tchernovi*, anteroposterior length to mediolateral width ratio is substantially greater than 2. In *K. mabokoensis*, it is 1.83. Care must be taken when comparing the dimensions of the suborbital fenestra—the shape of the fenestra changes ontogenetically and is subject to distortion in fossils—but we do not believe either is a factor here. The fenestra is narrow in both skulls referred to *K. tchernovi*, one of which (the type) is smaller than the *K. mabokoensis* type skull and the other of which (KNM-KA 68749) is much larger. Likewise, although the type is dorsoventrally compressed, KNM-KA 68749 is not, indicating that the narrow fenestra is not taphonomic.

Orientation of the external naris also distinguishes the two forms. The naris opens dorsally in *K. mabokoensis*. The naris appears to open anterodorsally in *K. tchernovi*, and the species was coded that way in our phylogenetic analyses, but its orientation is more complex (Figure 16). Posteriorly, the narial rim lies in a transverse plane. Its orientation changes to anterodorsal about halfway to its anterior margin, roughly at the same frontal plane as p4. The reoriented naris is more pronounced in the holotype from Loperot than in the larger skull from Karungu, but given the differences in size and degree of dorsolateral distortion, we believe the difference is intraspecific in nature.

5.3 | Relationships of *Kinyang* to other crocodylids

Kinyang mabokoensis preserves the choanal neck diagnostic of Osteolaeminae, albeit with a less prominent crest (Figure 6a). It also preserves a squamosal that extends onto the dorsal surface of the quadrate ramus anterolateral to the paroccipital process. The internal

choana lacks a septum. None of these could be confirmed for _K. tchernovi._

The single unambiguous synapomorphy _Kinyang_ that shares with other euthecodontins—a forked ectopterygoid maxillary ramus—is problematic. There are two reasons for this. First, its expression is variable within modern species of _Crocodylus_ (Brochu & Storrs, 2012). Most modern _Crocodylus_ specimens have forked ectopterygoids, but a few lack this feature.

Second, it is homoplastic among crocodyloids. Among crocodylines, extant species of _Crocodylus_ variably have forked maxillary rami, as do extinct _Crocodylus palaeindicus_ and _C. ossifragus_, but they are uniformly absent from Paleoafrican _Crocodylus_ and Turkana _C. checchiai_. They are also absent from _Mecistops_ and osteolaemines, with the exceptions of _Kinyang_, _Brochuchus pigotti_, and _Euthecodon brumpti_ Fourtau, 1920. (The condition in _Brochuchus parvidens_ is unknown, and it is absent in _Euthecodon arambourgii_ Ginsburg & Buffetaut, 1978, although only one specimen of _E. arambourgii_—the holotype—preserves this part of the skull.) Thus, although this character state diagnoses Euthecodontini in this analysis, the level of support it provides is less than robust.

We acknowledge that support for euthecodontin affinities of _Kinyang_ is weak. Moving _Kinyang_ to a basal position as the sister to all other osteolaemines increases tree length by only one step. Many alternative positions within Osteolaeminae—closer to osteolaemins or _"Crocodylus" gariepensis_, for example—only increase tree length by two steps. This obviously reflects the incomplete nature of several of the species included in our analysis, but it may also arise from the highly derived status of most osteolamines. Most deviate from what most might presume is the ancestral overall morphotype for Crocodylidae—that of a generalized form resembling most extant species of _Crocodylus_. Illumination is likely to come from inclusion of any pre-Miocene osteolaemines that might eventually come to light.

We are skeptical of the sister-group relationship between _Osteolaemus_ and _Kinyang_ recovered in our combined mtDNA-morphology analysis. We suspect lability on the part of _Voay_ is breaking up what would otherwise be a more inclusive Osteolaeminae. There is, nonetheless, morphological support for this assessment—in particular, both _Kinyang_ and _Osteolaemus_ have fewer teeth than most other crocodylids.

5.4 | Variability of caviconchal pits in crocodylids

The presence of an array of blind pits on the medial wall of the caviconchal recess has been considered diagnostic

for _Crocodylus_ (Brochu, 2000). They are absent from _Mecistops_ (Figure 8e), _Osteolaemus_ (Figure 8b), _Euthecodon_, _Voay_, and _"Crocodylus" gariepensis_, but present in all extant species of _Crocodylus_ (e.g., Figure 8d) and extinct _C. anthropophagus_ (Brochu, 2007; Brochu et al., 2010; Brochu & Storrs, 2012; McAliley et al., 2006). The smaller maxilla from Karungu lacks these pits (Figure 14c), though only the anteriormost part of the wall is preserved. Assuming the pits would have been absent along the length of the wall in the Karungu specimen, our analysis suggests that _K. mabokoensis_ acquired them independently.

A review of other putative osteolaemine specimens suggests a low level of variability in this feature. Pits as deep and extensive as those of _Crocodylus_ have never been observed in _Osteolaemus_, but the specimen figured by Brochu (2007) nevertheless reveals a pair of shallow depressions toward the anterior end of the recess (Figure 8b). Deep pits are absent in _Brochuchus pigotti_ specimens from Rusinga, but some shallow pits are present on one specimen (KNM-RU 52950) and three small pits are present at the anterior end of the recess in a left maxilla of _B. parvidens_ Cossette et al., 2020 from Maboko (KNM-MB 25736; CAB, personal observation).

More significantly, although most maxillae from the Early Miocene of Gebel Zelten (Libya) that may be referable to _Rimasuchus lloydi_ (Llinas Agrasar, 2004) bear at most two or three modest depressions at the posterior end of the recess (e.g., Figure 8d), the pits on one specimen (BRSUG 27279, Figure 8c) are quite deep, and shallow depressions can be found along the entire recess wall.

To test the impact of caviconchal pit polymorphism, we re-ran the analysis with a modified matrix. _Rimasuchus lloydi_, as used in previous analyses (e.g., Brochu, 2000; Brochu & Storrs, 2012), was based on a specimen from the Early Miocene of Wadi Moghra, which is where the type specimen was found (Fourtau, 1918). This time, we added character information from Gebel Zelten material housed at the University of Bristol and the Natural History Museum in London (Llinas Agrasar, 2004). The character expressing presence or absence of pits (character 101 in the matrix) was coded as polymorphic for this version of _R. lloydi_. The results were topologically and numerically identical to those when _R. lloydi_ is treated as unknown for this character.

Pneumatic structures in bones can be notoriously variable (e.g., Sherwood, 1999; O'Connor, 2006; Wedel & Taylor, 2013; Zurriaguz & Álvarez, 2014; Buchmann et al., 2021). Taylor and Wedel (in review) suggest that, for sauropods at least, this reflects variability in vasculature associated with pneumatic diverticula, but it could more simply reflect the comparatively late appearance of

osseous pneumatic structures in development; the air sacs and bones appear substantially before they contact each other. It is thus possible that what appears to be a complete absence in some taxa reflects comparatively low sample sizes more than a consistent lack of the feature. Further work is needed to assess the variability of these pits in the crocodylid rostrum.

5.5 | Variability in choanal morphology

On first blush, many specimens of *Crocodylus niloticus*—especially larger individuals—bear what appear to be circumchoanal crests (Figure 10f). The pterygoid surfaces are indeed elevated anterolateral to the choana in most crocodylids, which makes the choanal rim appear more prominent. One might thus conclude that these skulls share the derived state also found in *Osteolaemus* (Figure 10b,c,d), *Voay*, and *Kinyang* (Figure 10a).

In fact, the condition in *C. niloticus* differs from those of *Osteolaemus* and *Kinyang*, and it appears to be a matter of ontogenetic variation. In modern *Osteolaemus*, the crest—which is more prominent in *O. osborni* (Figure 10c) than in *O. tetraspis* (Figure 10b)—is present throughout posthatching ontogeny and evident in very small specimens (e.g., Figure 10d). In contrast, smaller specimens of *C. niloticus* lack this feature (Figure 10e). In larger individuals, it lies along the anterolateral sides of a triangular choana that opens nearly at the posterior margin of the pterygoids (Figure 10f). This reflects an ontogenetic shift in position of the choana rather than a change to the choanal rim per se.

Further work on this feature could prove enlightening. Triangular choanae appear to be less common in skulls we refer to *Crocodylus suchus* (CAB, personal observation), but our sample is much smaller with few large individuals, and in many cases, we refer such specimens to *C. suchus* based on their geographic origin. Triangular choanae sometimes occur in other species of *Crocodylus*, but a more complete survey is needed to properly assess variation in this structure.

5.6 | Crocodylian diversity and paleoecology in East Africa

Kinyang reinforces several observations about late Cenozoic crocodylians, and late Cenozoic continental vertebrates in general, in the EARS. First, it suggests uniformity in crocodylian faunas along the Kenya Rift. Sites in the TB and LVB share the same genera and, in at least one case (*K. tchernovi*), the same species. The only exception is *Euthecodon*, which has been reported from the LVB, but which does not appear in the TB until the Late Miocene. But *Euthecodon* is very rare in the LVP—only two fragments have been reported (Buffetaut, 1979; Tchernov & Couvering, 1978), and their referrals and provenance are debatable (CAB, personal observation). The rarity of *Euthecodon* from the southern Kenya Rift suggests its absence further north is a matter of sampling.

Second, it highlights the different phylogenetic compositions of crocodylian faunas before 15 Ma and after 7.2 Ma. Between the deposits at Loperot and Karungu and those at Maboko, we find the osteolaemines *Brochuchus* (Figure 1d) and *Kinyang*. Units in the Turkana Basin, starting with the Lower Member of the Nawata Formation, preserve *Crocodylus* (Figure 1f,g) and *Mecistops* (Figure 1e). The only lineages found throughout the Miocene in the Kenya Rift are "*Eogavialis*" (Figure 1h) and *Euthecodon* (Figure 1i), both of which are tubulirostrine. (Although living *Mecistops* have comparatively long and slender snouts [Figure 1c], this was not as true of the earliest-known occurrences of the genus in the Lower Nawata [Figure 1e; Storrs, 2003].)

Third, the skull of *Kinyang* has proportions unlike those of any other crocodylid, living or extinct, which implies functional or ecological attributes with no good modern analogue. A robust quantitative analysis is beyond the scope of this article, and there are several factors that make direct comparison difficult—most importantly, ontogenetic and ecophenotypic variation in craniomandibular proportion within extant crocodylian species (e.g., Drumheller et al., 2016; Foth et al., 2015, 2018; Kälin, 1933; Monteiro & Soares, 1997). Moreover, available skulls of *K. tchernovi* are incomplete, crushed, or both. Nevertheless, we note some visual differences.

At first glance, the snout of *Kinyang mabokoensis* appears to be short relative to skull length compared with those of most extant crocodylids. In fact, the snout is only slightly shortened in *Kinyang*, at least when skulls of similar size are compared—the ratio of rostrum length (tip of snout to front of orbits) to skull length (tip of snout to back of skull table) is 0.62, only slightly shorter than the average (0.68) for five modern *C. niloticus* skulls in the KNM, all collected at Lake Turkana and within 10% of the total length of the *K. mabokoensis* holotype skull.

The real difference is the relative width of the skull. For the *K. mabokoensis* holotype, the ratio of skull width at the quadrates to skull length is 0.72, and the ratio of skull width at m5 to skull length is 0.53. No extant crocodylid appears to have a skull that wide. The mean width/length ratios for the KNM sample of *C. niloticus* skulls are 0.52 at the quadrates and 0.28 at m5. The skulls of the smallest crocodylids (*Osteolaemus*) are deep and short, but not unusually wide; the width/length ratio for the holotype of *Osteolaemus osborni* (AMNH 10082) is

0.59 at the quadrates. *Osteolaemus* also shows additional modifications not seen in *Kinyang*, but shared with the unrelated smooth-fronted caimans (*Paleosuchus* Gray, 1862) of South America, such as restricted supratemporal fenestrae, labiolingually compressed teeth (though to a modest degree), and a heavily ossified compound palpebral. Better analogues might be found among alligatorids, such as the broad-snouted caiman (*Caiman latirostris* Daudin, 1801), whose skull is also unusually broad relative to its length (Bona & Desojo, 2011; Foth et al., 2018; Monteiro et al., 1997; Piras et al., 2009).

The broad, rounded snout seen in *Kinyang* falls within the ecomorphotypic range expected for a generalized semi-aquatic ambush predator (Brochu, 2001; Wilberg, 2017). A recent morphometric analysis of snout shapes across Crocodyliformes (Drumheller & Wilberg, 2020) further splits this broad-snouted morphotype into two functional groups. V-shaped snouts, such as that seen in *Crocodylus niloticus* (Figure 1a), correlate with diverse diets and prey species that range up to a similar size as the predator. Wider, less acute snouts, such as that of *Caiman latirostris*, correspond with a macro-generalist feeding strategy. These taxa are capable of taking diverse prey items that are as big or bigger than themselves. *Kinyang*'s robust dentition further supports this paleoecological interpretation (D'Amore et al., 2020).

The differences between early and late Neogene crocodile faunas in the Kenya rift are thus phylogenetic as well as morphological. Generalized crocodylids from the Early and early Middle Miocene are generally smaller, and the skull of the larger one is geometrically dissimilar from anything found in younger East African deposits. They are also unrelated to the generalized crocodylids seen in the Late Miocene through Holocene. What caused this turnover?

Cossette et al. (2020) suggested that this turnover was related to the trend in the EARS toward more expansive grasslands that began with the appearance of C_3-dominated grasslands driven by seasonal changes in rainfall in the Middle Miocene (Retallack, 1992; Retallack et al., 2002) and accelerated with the spread of C_4 grasslands in the Late Miocene and Pliocene (Cerling, 1992; Feakins et al., 2013; Feibel, 2011; Jacobs et al., 2010; Linder, 2017; Polissar et al., 2019; Saarinen et al., 2020; Wichura et al., 2015). These have been correlated with regional changes in nonmarine fauna; herbivorous mammal assemblages, for example, were dominated by browsers in the Early and Middle Miocene, but the proportion of grazers began rise later in the epoch and into the Pliocene (e.g., Bobe, 2006; Cerling et al., 2015; Hall & Cote, 2021; Leakey et al., 2011).

Modern *Osteolaemus* (Figure 1b) is generally limited to forested lowlands throughout western and central Africa (Eaton, 2010). The same is true for *Mecistops*, which falls out as an osteolaemine in most molecular phylogenetic analyses (e.g., Hekkala et al., 2021; McAliley et al., 2006; Meredith et al., 2011; Oaks, 2011; Pan et al., 2021). Assuming extinct osteolaemines shared similar environmental preferences, the regional reduction of woodland might have promoted their replacement by crocodylids more tolerant of open conditions.

The depositional systems at sites preserving *Kinyang* and *Brochuchus* all reflect mixed riparian woodlands and mixed open habitats that formed under comparatively dry conditions (Butts et al., 2018; Driese et al., 2016; Liutkus-Pierce et al., 2019; Lukens et al., 2017; Michel et al., 2020; Retallack et al., 2002). But living dwarf crocodiles are not restricted to closed-canopy rain forests; they can be found in riparian woodlands and seasonal wetlands (e.g., Eaton, 2010; Ceríaco & de Sá, 2018; Amoah et al., 2021). Thus, the kinds of biomes that dominated Early to Middle Miocene sites preserving generalized osteolaemines might not reflect different ecological preferences from modern *Osteolaemus*.

There are several caveats that must be borne in mind when assessing the link between Miocene osteolaemines and vegetational change. The most important is the substantial stratigraphic gap between around 15 Ma and around 7 Ma. The last appearances of *Kinyang* and *Brochuchus* roughly coincide with the end of the Miocene Climatic Optimum and the onset of lower global average temperatures and a drop in atmospheric CO_2 content (Westerhold et al., 2020). The EARS experienced a trend toward drier conditions following this event, which would have created conditions favorable to grasslands. But because we do not know how closely the last appearance datum for *Kinyang* approximates its extinction, the relationship between the loss of generalized osteolaemines and environmental change prompted by the end of the Miocene Climatic Optimum is less than robust.

This gap leads to several other complications. Regional drying in the EARS might have been driven by weakening of summer monsoons as the Tethys Sea shrank during the Late Miocene (Zhang et al., 2014). Reductions in atmospheric CO_2 may have played a major role in driving the expansion of grasslands, even in the absence of xerification (Polissar et al., 2019). Each of these would reflect climatic changes substantially after the end of the Miocene Climatic Optimum.

Moreover, climate is not the only plausible factor for Miocene crocodylid faunal turnover. Most tectonic activity associated with faulting of the Kenya Rift is thought to have begun at around this time. This led to the formation of large, deep rift lakes and changes in fluvial drainage patterns (Feibel, 2011; Wichura et al., 2015). There

were also major volcanic events beginning at around 12 Ma (Rooney, 2020). Any of these, with or without climate change, could have driven changes in crocodylid faunas in the EARS.

Yet another complication is *Mecistops*. Like modern *Osteolaemus*, it prefers forested wetlands (Kofron, 1992; Kouman et al., 2021; Shirley, 2010). In the Kenya Rift, it is only known from sites no older than the Lower Nawata (Storrs, 2003). *Mecistops* is less common at Turkana Basin sites than other co-occurring crocodylids (CAB, personal observation), and so it might not represent the prevailing ecosystems of the relevant sequences in the same way as *Euthecodon* and Paleoafrican *Crocodylus*, but there does appear to be a conflict with the expected pattern based on regional vegetational change.

However, patterns of extant crocodylian diversity are driven by a complex array of environmental factors, including direct and indirect effects of vegetation. Plants provide food and habitat for prey species; contribute to landscape structure and chemistry; and supply cover, concealment, and nesting materials to crocodylians themselves. That said, few crocodylian taxa would be described as vegetative specialists (Somaweera et al., 2019). An exception to this seems potentially relevant to the paleontological discussion at hand: the nesting ecology of *Mecistops* and *Osteolaemus*.

Crocodylian nest types can differ between and even within species, with preferences for mount or pit style nests varying across populations and environments. That said, all extant crocodylians generally prefer concealed, elevated areas that simultaneously keep developing eggs safely above the water table until hatching while also providing the adults with easy access to water. Most species will incorporate both sediment and vegetation into their nests, and the plant material used can have a large impact on overall size and appearance as the vegetation provides protection from predators and the sun and the decomposing organics produce heat, which warms and stabilizes the internal temperatures of the nests (e.g., Joanen & McNease, 1989; Murray et al., 2020; Platt et al., 1995; Thorbjarnarson, 1996; Thorbjarnarson & Wang, 2010; Webb et al., 1977, 1983). The loss of sources of appropriate nest-building vegetation can prevent or displace successful nesting (Somaweera et al., 2019), and smaller-scale vegetative changes that affect nest structural integrity and microclimate have been shown to decrease nesting success, due to either inadequate protection of incubating eggs or to temperature fluctuations beyond the tolerances of the developing embryos (Somaweera et al., 2019; Thorbjarnarson & Wang, 2010).

Both *Mecistops* and *Osteolaemus* prefer to live in forested areas, though *Mecistops* nests have been found in more open woodland and disturbed or cultivated areas than *Osteolaemus* (Shirley, 2010; Shirley et al., 2009; Waitkuwait, 1986). Both exhibit specializations related to nest building that are strongly linked with the vegetation present in their environments. Both build mostly mound-style nests, constructed nearly entirely of decaying vegetation, particularly leaf litter, the size and shape of which are governed by a combination of available vegetation and the height of the water table (Murray et al., 2020; Shirley, 2010; Waitkuwait, 1986). In areas where the two taxa are sympatric, nesting is not syntopic. It is partitioned both temporally and spatially; *Mecistops* nests are typically found parallel to the riverbanks while *Osteolaemus* nests in swampier regions, further from sources of flowing water (Waitkuwait, 1986).

This reproductive specialization suggests one driver of the changeover in crocodylian communities preserved in the EARS. The earlier, forested environments with abundant rivers and swampy areas would have been within the ecological tolerances of both *Mecistops* and *Osteolaemus*, but as the region dried, giving way to grasslands and drainage systems dominated by lakes, the new environment may have favored taxa with more flexible reproductive requirements, including *Crocodylus*, a mound or hole-style nest builder with more variable vegetative preferences, and gharials, whose communal nests are largely sediment, rather than plant, based (Lang & Kumar, 2013; Murray et al., 2020; Vashistha et al., 2021). That *Mecistops* nests are more likely than those of *Osteolaemus* to be found in more open settings may explain its presence in the Late Miocene and Plio-Pleistocene.

That said, any definitive link between fossil crocodylid faunal content and vegetational change requires additional testing, much of which is reliant on collection of new crocodylids in the EARS. In particular, fossils in the Kenya Rift from within the temporal gap separating Maboko and Lothagam could shed considerable light on this issue by helping narrow down the stratigraphic interval within which osteolaemines were replaced by crocodylines. So would a more precise assessment of the paleocology of Late Miocene and Plio-Pleistocene sites preserving crocodylids.

AUTHOR CONTRIBUTIONS

Christopher A. Brochu: Conceptualization (lead); data curation (lead); formal analysis (equal); funding acquisition (lead); investigation (lead); methodology (equal); project administration (lead); supervision (lead); validation (lead); visualization (lead); writing – original draft (lead); writing – review and editing (lead). **Ane de Celis:** Formal analysis (equal); funding acquisition (supporting); investigation (supporting); methodology (equal); writing – original draft (supporting). **Amanda**

J. Adams: Data curation (supporting); funding acquisition (supporting); investigation (supporting). **Stephanie K. Drumheller:** Data curation (supporting); formal analysis (supporting); funding acquisition (equal); investigation (supporting); writing – original draft (supporting); writing – review and editing (equal). **Jennifer H. Nestler:** Data curation (supporting); formal analysis (supporting); funding acquisition (supporting); investigation (supporting); writing – original draft (supporting). **Brenda R. Benefit:** Data curation (equal); funding acquisition (equal); investigation (supporting); writing – original draft (supporting); writing – review and editing (equal). **Aryeh Grossman:** Data curation (equal); funding acquisition (equal); investigation (supporting); writing – original draft (supporting); writing – review and editing (equal). **Francis Kirera:** Data curation (supporting); writing – original draft (supporting); writing – review and editing (supporting). **Thomas Lehmann:** Data curation (equal); funding acquisition (equal); investigation (supporting); writing – original draft (supporting); writing – review and editing (equal). **Cynthia Liutkus-Pierce:** Data curation (equal); funding acquisition (equal); writing – original draft (supporting); writing – review and editing (supporting). **Fredrick K. Manthi:** Data curation (equal). **Monte L. McCrossin:** Data curation (equal); funding acquisition (equal); investigation (supporting); writing – original draft (supporting); writing – review and editing (equal). **Kieran P. McNulty:** Data curation (equal); funding acquisition (equal); writing – original draft (equal); writing – review and editing (supporting). **Rose Nyaboke Juma:** Data curation (equal).

ORCID

Christopher A. Brochu https://orcid.org/0000-0003-4044-8371

REFERENCES

Adams, A. J. (2020). Reassessment of Cenozoic longirostrine crocodiles of East Africa. In *Earth and environmental sciences* (p. 525). University of Iowa.

Akaike, H. (1973). Information theory and an extension of the maximum likelihood principle. In B. N. Petrov & F. Csáki (Eds.), *2nd international symposium on information theory* (pp. 267–281). Budapest.

Amoah, E., Danquah, E., & Ross, J. P. (2021). Nesting ecology of West African dwarf crocodiles in a heavily disturbed landscape in Chirehin, Ghana. *Hindawi*, *2021*, 1–11.

Andrews, P., Meyer, G. E., Pilbeam, D. R., Van Couvering, J. A., & Van Couvering, J. A. H. (1981). The Miocene fossil beds of Maboko Island, Kenya: Geology, age, taphonomy and palaeontology. *Journal of Human Evolution*, *10*, 35–48.

Arambourg, C. (1947). Contribution a l'étude géologique et paléontologique du Bassin du Lac Rodolphe et de la Basse Vallée de l'Omo. In C. Arambourg (Ed.), *Mission Scientifique de l'Omo 1932–1933, Tome I: Geologie - Anthropologie* (pp. 231–562). Muséum National d'Histoire Naturelle.

Arney, I. D., Benefit, B. R., McCrossin, M. L., & Kingston, J. D. (In press). Herbivore dietary ecology of the middle Miocene Maboko formation, Kenya. *Palaeogeography, Palaeoclimatology, Palaeoecology*.

Arney, I. D., Maclatchy, L., Benefit, B. R., McCrossin, M. L., & Kingston, J. D. (2018). Environmental change and African early to middle Miocene catarrhine evolution. *American Journal of Physical Anthropology*, *165*, 12–13.

Azzarà, B., Boschian, G., Brochu, C. A., Delfino, M., Iurino, D. A., Kimambo, J. S., Manzi, G., Masao, F., Menconero, S.,

Njau, J. K., & Cherin, M. (2021). A new cranium of *Crocodylus anthropophagus* from Olduvai Gorge, northern Tanzania. *Revista Italiana di Paleontologia e Stratigrafia*, 127, 275–295.

Benefit, B. R. (1999). *Victoriapithecus*: The key to Old World monkey and catarrhine origins. *Evolutionary Anthropology*, 7, 155–174.

Benefit, B. R., & McCrossin, M. L. (1989). New primate fossils from the middle Miocene of Maboko Island, Kenya. *Journal of Human Evolution*, 18, 493–497.

Bennett, E. T. (1835). Crocodilus leptorhynchus. *Proceedings of the Zoological Society of London*, 3, 128–132.

Benton, M. J., & Clark, J. M. (1988). Archosaur phylogeny and the relationships of the Crocodylia. In M. J. Benton (Ed.), *The phylogeny and classification of the Tetrapods* (pp. 295–338). Clarendon Press.

Berg, D. E. (1966). Die Krokodile, insbesondere *Asiatosuchus* und aff. *Sebecus*?, aus dem Eozän von Messel bei Darmstadt/Hessen. *Abhandlungen des Hessischen Landesamtes für Bodenforschung*, 52, 1–105.

Bergner, A. G. N., Strecker, M. R., Trauth, M. H., Deino, A. L., Gasse, F., Blisniuk, P., & Dühnforth, M. (2009). Tectonic and climatic control on evolution of rift lakes in the Central Kenya rift, East Africa. *Quaternary Science Reviews*, 28, 2804–2816.

Bobe, R. (2006). The evolution of arid ecosystems in eastern Africa. *Journal of Arid Environments*, 66, 564–584.

Bona, P., & Desojo, J. B. (2011). Osteology and cranial musculature of *Caiman latirostris* (Crocodylia: Alligatoridae). *Journal of Morphology*, 272, 780–795.

Boschetto, H. B., Brown, F. H., & McDougall, I. (1992). Stratigraphy of the Lothidok range, northern Kenya, and K/Ar ages of its Miocene primates. *Journal of Human Evolution*, 22, 47–71.

Brochu, C. A. (2000). Phylogenetic relationships and divergence timing of *Crocodylus* based on morphology and the fossil record. *Copeia*, 2000, 657–673.

Brochu, C. A. (2001). Crocodylian snouts in space and time: Phylogenetic approaches toward adaptive radiation. *American Zoologist*, 41, 564–585.

Brochu, C. A. (2003). Phylogenetic approaches toward crocodylian history. *Annual Review of Earth and Planetary Sciences*, 31, 357–397.

Brochu, C. A. (2006). A new miniature horned crocodile from the quaternary of Aldabra atoll, western Indian Ocean. *Copeia*, 2006, 149–158.

Brochu, C. A. (2007). Morphology, relationships and biogeographic significance of an extinct horned crocodile (Crocodylia, Crocodylidae) from the quaternary of Madagascar. *Zoological Journal of the Linnean Society*, 150, 835–863.

Brochu, C. A. (2020). Pliocene crocodiles from Kanapoi, Turkana Basin, Kenya. *Journal of Human Evolution*, 140, 102410.

Brochu, C. A., Njau, J. K., Blumenschine, R. J., & Densmore, L. D. (2010). A new horned crocodile from the Plio-Pleistocene hominid sites at Olduvai Gorge, Tanzania. *PLoS One*, 5, e9333.

Brochu, C. A., & Storrs, G. W. (2012). A giant crocodile from the Plio-Pleistocene of Kenya, the phylogenetic relationships of Neogene African crocodylines, and the antiquity of *Crocodylus* in Africa. *Journal of Vertebrate Paleontology*, 32, 587–602.

Brown, C. M., Van Buren, C. S., Larson, D. W., Brink, K. S., Campione, N. E., Vavrek, M. J., & Evans, D. C. (2015). Tooth counts through growth in diapsid reptiles: Implicatons for interpreting individual and size-related variation in the fossil record. *Journal of Anatomy*, 226, 322–333.

Buchanan, L. A. (2009). *Kambara taraina* sp. nov. (Crocodylia, Crocodyloidea), a new Eocene mekosuchine from Queensland, Australia, and a revision of the genus. *Journal of Vertebrate Paleontology*, 29, 473–486.

Buchmann, R., Holgado, B., Sobral, G., dos Santos, A. L., & Rodrigues, T. (2021). Quantitative assessment of the vertebral pneumaticity in an anhanguerid pterosaur using micro-CT scanning. *Scientific Reports*, 11, 18718.

Buffetaut, E. (1979). Présence du crocodilien *Euthecodon* dans le Miocène inférieur d'Ombo (Golfe de Kavirondo, Kenya). *Bulletin de la Société Géologique de France*, 21, 321–322.

Buffetaut, E. (1982). Radiation évolutive, paléoécologie et biogéographie des crocodiliens mesosuchiens. *Memoires de la Societé Geologique de France*, 60, 1–88.

Butts, C., Cote, S., & Kingston, J. (2018). Reconstructing the paleoenvironments of Kalodirr and Moruorot, Kenya using stable carbon isotopes. *Vertebrate Anatomy Morphology Paleontology*, 5, 12–13.

Ceríaco, L. M. P., & de Sá, S. A. C. (2018). The genus *Osteolaemus* (Crocodylidae) in Angola and a new southernmost record for the genus. *Herpetology Notes*, 11, 337–341.

Cerling, T. E. (1992). Development of grasslands and savannas in East Africa during the Neogene. *Palaeogeography, Palaeoclimatology, Palaeoecology*, 97, 241–247.

Cerling, T. E., Andanje, S. A., Blumenthal, S. A., Brown, F. H., Chritz, K. L., Harris, J. M., Hart, J. A., Kirera, F. M., Kaleme, P., Leakey, L. N., Leakey, M. G., Levin, N. E., Manthi, F. K., Passey, B. H., & Uno, K. T. (2015). Dietary changes of large herbivores in the Turkana Basin, Kenya from 4 to 1 ma. *Proceedings of the National Academy of Sciences of the United States of America*, 112, 11467–11472.

Chorowicz, J. (2005). The east African rift system. *Journal of African Earth Sciences*, 43, 379–410.

Conrad, J. A., Jenkins, K., Lehmann, T., Manthi, F. K., Peppe, D. J., Nightingale, S., Cossette, A., Dunsworth, H. M., Harcourt-Smith, W. E. H., & McNulty, K. P. (2013). New specimens of 'Crocodylus' pigotti (Crocodylidae) from Rusinga Island, Kenya, and generic reallocation of the species. *Journal of Vertebrate Paleontology*, 33, 629–646.

Cope, E. D. (1861). List of the recent species of emydosaurian reptiles in the Museum of the Academy of natural sciences. *Proceedings of the Academy of Natural Sciences of Philadelphia*, 12, 549–550.

Cossette, A. P., Adams, A. J., Drumheller, S. K., Nestler, J. H., Benefit, B. R., McCrossin, M. L., Manthi, F. K., Nyaboke Juma, R., & Brochu, C. A. (2020). A new crocodylid from the middle Miocene of Kenya and the timing of crocodylian faunal change in the late Cenozoic of Africa. *Journal of Paleontology*, 94, 1165–1179.

Cuvier, G. (1825). *Recherches Sur les Ossemens Fossiles, où l'On Rétablit les Caractères de Plusieurs Animaux Dont les Révolutions du Globe Ont Détruit les Espèces* (2nd ed.). G. Doufour et Ed. D'Ocagne.

D'Amore, D. C., Harmon, M., Drumheller, S. K., & Testin, J. J. (2020). Quantitative heterodonty in Crocodylia: Assessing size and shape across modern and extinct taxa. *PeerJ*, 7, e6485.

Darriba, D., Taboada, G. L., Doallo, R., & Posada, D. (2012). jModelTest 2: More models, new heuristics and parallel computing. *Nature Methods*, 9, 772.

Daudin, F. M. (1801). *Histoire Naturelle, Générale et Particulière des Reptiles* (Vol. II). Imprimerie de F. Dufart.

Delfino, M., Iurino, D. A., Mercurio, B., Piras, P., Rook, L., & Sardella, R. (2020). Old African fossils provide new evidence for the origin of the American crocodiles. *Scientific Reports*, *10*, 11127.

Drake, R. E., Van Couvering, J. A., Pickford, M. H., Curtis, G. H., & Harris, J. A. (1988). New chronology for the early Miocene mammalian faunas of Kisingiri, western Kenya. *Journal of the Geological Society*, *145*, 479–491.

Driese, S. G., Peppe, D. J., Beverly, E. J., DiPietro, L. M., Arellano, L. N., & Lehmann, T. (2016). Paleosols and paleoenvironments of the early Miocene deposits near Karungu, Lake Victoria, Kenya. *Palaeogeography, Palaeoclimatology, Palaeoecology*, *443*, 167–182.

Drumheller, S. K., & Wilberg, E. W. (2020). A synthetic approach for assessing the interplay of form and function in the crocodyliform snout. *Zoological Journal of the Linnean Society*, *188*, 507–521.

Drumheller, S. K., Wilberg, E. W., & Sadleir, R. W. (2016). The utility of captive animals in actualistic research: A geometric morphometric exploration of the tooth row of *Alligator mississippiensis* suggesting ecophenotypic influences and functional constraints. *Journal of Morphology*, *277*, 866–878.

Eaton, M. J. (2010). Dwarf crocodile *Osteolaemus tetraspis*. In S. C. Manolis & C. Stevenson (Eds.), *Crocodiles: Status survey and conservation action plan* (3rd ed., pp. 127–132). IUCN Crocodile Specialist Group.

Falconer, H. (1859). *Descriptive catalogue of fossil remains of vertebrata from the Sewalik Hills, the Nerbudda, Perim Island, etc. in the Museum of the Asiatic Society of Bengal*. C. B. Lewis, Baptist Mission Press.

Feakins, S. J., Levin, N. E., Liddy, H. M., Sieracki, A., Eglinton, T. I., & Bonnefille, R. (2013). Northeast African vegetation change over 12 m.y. *Geology*, *41*, 295–298.

Feibel, C. S. (2011). A geological history of the Turkana Basin. *Evolutionary Anthropology*, *20*, 206–216.

Feibel, C. S., & Brown, F. H. (1991). Age of the primate-bearing deposits on Maboko Island, Kenya. *Journal of Human Evolution*, *21*, 221–225.

Foth, C., Bona, P., & Desojo, J. B. (2015). Intraspecific variation in the skull morphology of the black caiman *Melanosuchus Niger* (Alligatoridae, Caimaninae). *Acta Zoologica*, *96*, 1–13.

Foth, C., Fernandez Blanco, M. V., Bona, P., & Scheyer, T. (2018). Cranial shape variation in jacarean caimanines (Crocodylia, Alligatoroidea) and its implications in the taxonomic status of extinct species: The case of *Melanosuchus fisheri*. *Journal of Morphology*, *279*, 259–273.

Fourtau, R. (1918). *Contribution à l'etude des vertebres miocènes de l'Egypte*. Egypt Survey Department.

Fourtau, R. (1920). Supplément. In R. Fourtau (Ed.), *Contribution à l'etude des vertebres miocènes de l'Egypte* (pp. 111–121). Egypt Survey Department.

Gilmore, C. W. (1910). *Leidyosuchus sternbergii*, a new species of crocodile from the cretaceous beds of Wyoming. *Proceedings of the United States National Museum*, *38*, 485–502.

Ginsburg, L., & Buffetaut, E. (1978). *Euthecodon arambourgii* n. sp., et l'evolution du genre *Euthecodon*, crocodilien du Néogène d'Afrique. *Géologie Méditerranéene*, *5*, 291–302.

Gmelin, J. (1789). *Linnei Systema Naturae*. G. E. Beer.

Gray, J. E. (1825). A synopsis of the genera or reptiles and Amphibia, with a description of some new species. *Annals of Philosophy*, *10*, 193–217.

Gray, J. E. (1844). *Catalogue of tortoises, crocodilians, and Amphisbaenians in the collection of the British museum*. British Museum (Natural History).

Gray, J. E. (1862). A synopsis of the species of crocodiles. *Annals and Magazine of Natural History*, *10*, 265–274.

Groh, S. S., Upchurch, P., Barrett, P. M., & Day, J. J. (2020). The phylogenetic relationships of neosuchian crocodiles and their implications for the convergent evolution of the longirostrine condition. *Zoological Journal of the Linnean Society*, *188*, 473–506.

Hall, A. S., & Cote, S. (2021). Ruminant mesowear reveals consistently browse-dominated diets throughout the early and middle Miocene of eastern Africa. *Palaeogeography, Palaeoclimatology, Palaeoecology*, *567*, 110253.

Harris, J. M., Leakey, M. G., Cerling, T. E., & Winkler, A. J. (2003). Early Pliocene tetrapod remains from Kanapoi, Lake Turkana Basin, Kenya. *Contributions in Science of the Los Angeles County Museum*, *498*, 39–113.

Hekkala, E., Gatesy, J., Narachania, A., Meredith, R., Russello, M. A., Aardema, M., Jensen, E., Montanari, S., Brochu, C. A., Norell, M., & Amato, G. (2021). Ancient DNA illuminates the evolutionary history of the extinct Holocene crocodile of Madagascar, *Voay robustus*. *Nature Communications Biology*, *4*, 505.

Hekkala, E., Shirley, M. H., Amato, G., Austin, J. D., Charter, S., Thorbjarnarson, J., Vliet, K. A., Houck, M. L., DeSalle, R., & Blum, M. J. (2011). An ancient icon reveals new mysteries: Mummy DNA resurrects a cryptic species within the NIle crocodile. *Molecular Ecology*, *20*, 4199–4215.

Huelsenbeck, J. P., & Ronquist, F. (2001). MrBayes. In, 2.01 ed. Rochester, NY.

Iijima, M. (2017). Assessment of trophic ecomorphology in non-alligatoroid crocodylians and its adaptive and taxonomic implications. *Journal of Anatomy*, *231*, 192–211.

Jacobs, B. F., Pan, A. D., & Scotese, C. R. (2010). A review of the Cenozoic vegetation history of Africa. In L. Werdelin & W. J. Sanders (Eds.), *Cenozoic mammals of Africa* (pp. 57–72). University of California Press.

Joanen, T., & McNease, L. L. (1989). Ecology and physiology of nesting and early development of the American alligator. *American Zoologist*, *29*, 987–998.

Joleaud, M. L. (1930). Les crocodiliens du pliocène d'eau douce de Omo. In *Livre Jubilaire, Centenaire de la Société Géologique de France* (pp. 411–429). Société Géologique de France.

Jouve, S. (2007). Taxonomic revision of the dyrosaurid assemblage (Crocodyliformes:Mesoeucrocodylia) from the Paleocene of the Iullemmeden Basin, West Africa. *Journal of Paleontology*, *81*, 163–175.

Kälin, J. A. (1933). Beiträge zur vergleichenden Osteologie des Crocodilidenschädels. *Zoologische Jahrbücher*, *57*, 535–714.

Kofron, C. P. (1992). Status and habitats of the three African crocodiles in Liberia. *Journal of Tropical Ecology*, *8*, 265–273.

Kouman, C. Y., Ebome, A. E. A., Ahizi, M. N., Ouattara, M., Ouattara, A., Fairet, E., & Shirley, M. H. (2021). Space use and social interactions of central African slender-snouted crocodiles

Mecistops leptorhynchus (Bennett, 1835) in Loango National Park, Gabon. *African Journal of Ecology*, 59, 866–879.

Lang, J. W., & Kumar, P. J. (2013). Behavioral ecology of gharial on the Chambal River, India. In I. C. W. Group (Ed.), *World Crocodile Conference: Proceedings of the 22nd Working Meeting of the IUCN SSC Crocodile Specialist Group* (pp. 42–52). Gland, Switzerland, International Union for Conservation of Nature.

Laurenti, J. N. (1768). *Specimen Medicum, Exhibens Synopsin Reptilium Emendatum cum Experimentatis Circa Venena et Antiodota Reptilium Austriacorum*. J. T. de Trattnern.

Leaché, A. D., Rödel, M.-O., Linkem, C. W., Diaz, R. E., Hillers, A., & Fujita, M. K. (2006). Biodiversity in a forest Island: Reptiles and amphibians of the west African Togo Hills. *Amphibian and Reptile Conservation*, 4, 22–45.

Leakey, M., Grossman, A., Gutiérrez, M., & Fleagle, J. G. (2011). Faunal change in the Turkana Basin during the late Oligocene and Miocene. *Evolutionary Anthropology*, 20, 238–253.

Lee, M. S. Y., & Yates, A. M. (2018). Tip-dating and homoplasy: Reconciling the shallow molecular divergences of modern gharials with their long fossil record. *Proceedings of the Royal Society of London B*, 285, 20181071.

Lewis, P. O. (2001). A likelihood approach to estimating phylogeny from discrete morphological character data. *Systematic Biology*, 50, 913–925.

Linder, H. P. (2017). East African Cenozoic vegetation history. *Evolutionary Anthropology*, 26, 300–312.

Liutkus-Pierce, C. M., Takashita-Bynum, K. K., Beane, L. A., Edwards, C. T., Burns, O. E., Mana, S., Hemming, S., Grossman, A., Wright, J. D., & Kirera, F. M. (2019). Reconstruction of the early Miocene critical zone at Loperot, southwestern Turkana, Kenya. *Frontiers in Ecology and Evolution*, 77, 1–20.

Llinás Agrasar, E. (2004). Crocodile remains from the Burdigalian (lower Miocene) of Gebel Zelten (Libya). *Geodiversitas*, 26, 309–321.

Lukens, W. E., Lehmann, T., Peppe, D. J., Fox, D. L., Driese, S. G., & McNulty, K. P. (2017). The early Miocene critical zone at Karungu, western Kenya: An equatorial, open habitat with few primate remains. *Frontiers in Ecology and Evolution*, 5, 1–21.

Maccagno, A. M. (1947). Descrizione di una nuova specie di "*Crocodilus*" del giacimento di Sahabi (Sirtica). *Atti della Reale Accademia Nazionale dei Lincei: Memorie della Classe di Scienze fisiche, Mathematiche e Naturale*, 8(1), 63–96.

Marsh, O. C. (1871). Notice of some new fossil reptiles from the cretaceous and tertiary formations. *American Journal of Science*, 3(1), 447–459.

Massonne, T., Vasilyan, D., Rabi, M., & Böhme, M. (2019). A new alligatoroid from the Eocene of Vietnam highlights an extinct Asian clade independent from extant *Alligator sinensis*. *PeerJ*, 7, e7562.

Mayr, G. (2014). On the middle Miocene avifauna of Maboko Island, Kenya. *Geobios*, 47, 133–146.

McAliley, L. R., Willis, R. E., Ray, D. A., White, P. S., Brochu, C. A., & Densmore, L. D. (2006). Are crocodiles really monophyletic? - evidence for subdivisions from sequence and morphological data. *Molecular Phylogenetics and Evolution*, 39, 16–32.

McCollum, M. S., Peppe, D. J., McNulty, K. P., Dunsworth, H. M., Harcourt-Smith, W. E. H., & Andrews, A. L. (2013).

Magnetostratigraphy of the earlyi Miocene Hiwegi formation (Rusinga Island, Lake Victoria, Kenya). *Geological Society of America Abstracts with Programs*, 45, 12.

Meredith, R. W., Hekkala, E. R., Amato, G., & Gatesy, J. (2011). A phylogenetic hypothesis for *Crocodylus* (Crocodylia) based on mitochondrial DNA: Evidence for a trans-Atlantic voyage from Africa to the New World. *Molecular Phylogenetics and Evolution*, 60, 183–191.

Michel, L. A., Lehmann, T., McNulty, K. P., Driese, S. G., Dunsworth, H. M., Fox, D. L., Harcourt-Smith, W. E. H., Jenkins, K., & Peppe, D. J. (2020). Sedimentological and palaeoenvironmental study from Waregi Hill in the Hiwegi formation (early Miocene) on Rusinga Island, Lake Victoria, Kenya. *Sedimentology*, 67, 3567–3594.

Molnar, R. E. (1981). Pleistocene ziphodont crocodilians of Queensland. *Records of the Australian Museum*, 33, 803–835.

Monteiro, L. R., Cavalcanti, M. J., & Sommer, H. J. S. (1997). Comparative ontogenetic shape changes in the skull of *Caiman* species (Crocodylia, Alligatoridae). *Journal of Morphology*, 231, 53–62.

Monteiro, L. R., & Soares, M. (1997). Allometric analysis of the ontogenetic variation and evolution of the skull in *Caiman* Spix, 1825 (Crocodylia: Alligatoridae). *Herpetologica*, 53, 62–69.

Mook, C. C. (1940). A new fossil crocodilian from Mongolia. *American Museum Novitates*, 1097, 1–3.

Mook, C. C. (1941). A new crocodilian from the Lance Formation. *American Museum Novitates*, 1128, 1–5.

Müller, S., & Schlegel, H. (1844). Over de Krokodillen van den Indischen Archipel. In C. J. Temminck (Ed.), *Verhandlingen over de Natuurlijke Geschiedenis der Nederlandsche Overzeesche Bezittengen, Door de Leden der Natuurkundige Commissie in Ost-Indië en Andere Schrijvers* (pp. 1–70). Luchtmans & van der Hoek.

Murray, C. M., Crother, B. I., & Doody, J. S. (2020). The evolution of crocodilian nesting ecology. *Ecology and Evolution*, 10, 131–149.

O'Connor, P. M. (2006). Postcranial pneumaticity: An evaluation of soft-tissue influences on the postcranial skeleton and the reconstruction of pulmonary anatomy in archosaurs. *Journal of Morphology*, 267, 1199–1226.

Oaks, J. R. (2011). A time-calibrated species tree of Crocodylia reveals a recent radiation of the true crocodiles. *Evolution*, 65, 3285–3297.

Pan, T., Miao, J.-S., Zhang, H.-B., Yan, P., Lee, P.-S., Jiang, X.-Y., Ouyang, J.-H., Deng, Y.-P., Zhang, B.-W., & Wu, X.-B. (2021). Near-complete phylogeny of extant Crocodylia (Reptilia) using mitogenome-based data. *Zoological Journal of the Linnean Society*, 191, 1075–1089.

Peppe, D. J., Deino, A. L., Driese, S. G., Dunsworth, H. M., Fox, D. L., Harcourt-Smith, W. E. H., Jenkins, K., & Lehmann, T. (2017). Revised geochronology of the early Miocene faunas from Rusinga Island and Mfangano Island (Lake Victoria, Kenya): Implications for Miocene hominoid evolution and faunal succession. *American Journal of Physical Anthropology*, 162, 312–313.

Peppe, D. J., Deino, A. L., McNulty, K. P., Lehmann, T., Harcourt-Smith, W. E. H., Dunsworth, H. M., & Fox, D. L. (2011). New age constraints on the early Miocene faunas of Ruinga and Mfangano Islands (Lake Victoria, Kenya). *American Journal of Physical Anthropology*, 144(Suppl. 52), 237.

Pickford, M. (1981). Preliminary Miocene mammalian biostratigraphy for western Kenya. *Journal of Human Evolution*, *10*, 73–97.

Pickford, M. (1983). Sequence and environments of the lower and middle Miocene hominoids of western Kenya. In R. L. Ciochon & R. S. Corruccini (Eds.), *New interpretations of ape and human ancestry* (pp. 421–439). Plenum Press.

Pickford, M. (1986). Sedimentation and fossil preservation in the Nyanza Rift System, Kenya. *Geological Society Special Publication*, *25*, 345–362.

Pickford, M. (2003). A new species of crocodile from early and middle Miocene deposits of the lower Orange River valley, Namibia, and the origins of the Nile crocodile *(Crocodylus niloticus)*. *Geological Survey of Namibia Memoir*, *19*, 51–65.

Piras, P., Teresi, L., Buscalioni, A. D., & Cubo, J. (2009). The shadow of forgotten ancestors differently constrains the fate of Alligatoroidea and Crocodyloidea. *Global Ecology and Biogeography*, *18*, 30–40.

Platt, S. G., Hastings, R. W., & Brantley, C. G. (1995). Nesting ecology of the American alligator in southeastern Louisiana. *Proceedings of the Annual Conference of Southeastern Fish and Wildlife Agencies*, *49*, 629–639.

Polissar, P. J., Rose, C., Uno, K. T., Phelps, S. R., & DeMenocal, P. B. (2019). Synchronous rise of African C_4 ecosystems 10 million years ago in the absence of aridification. *Nature Geoscience*, *12*, 657–660.

Posada, D. (2008). jModelTest: phylogenetic model averaging. *Molecular Biology and Evolution*, *25*, 1253–1256.

Rambaut, A., Drummond, A., Xie, D., Baele, G., & Suchard, M. A. (2018). Posterior summarisation in Bayesian phylogenetics using tracer 1.7. *Systematic Biology*, *67*, 901–904.

Retallack, G. J. (1992). Middle Miocene plants from Fort Ternan (Kenya) and evolution of African grasslands. *Paleobiology*, *18*, 383–400.

Retallack, G. J., Wynn, J. G., Benefit, B. R., & McCrossin, M. L. (2002). Paleosols and paleoenvironments of the middle MIocene, Maboko Formation, Kenya. *Journal of Human Evolution*, *42*, 659–703.

Riley, J., & Huchzermeyer, F. W. (1999). African dwarf crocodiles in the Likouala swamp forests of The Congo Basin: Habitat, density, and nesting. *Copeia*, *1999*, 313–320.

Rio, J. P., & Mannion, P. D. (2021). Phylogenetic analysis of a new morphological dataset elucidates the evolutionary history of Crocodylia and resolves the long-standing gharial problem. *PeerJ*, *9*, e12094.

Ronquist, F., & Huelsenbeck, J. P. (2003). MrBayes 3: Bayesian phylogenetic inference under mixed models. *Bioinformatics*, *19*, 1572–1574.

Rooney, T. O. (2020). The Cenozoic magmatism of East Africa: Part II – rifting of the mobile belt. *Lithos*, *360-361*, 105291.

Saarinen, J., Mantzouka, D., & Sakala, J. (2020). Aridity, cooling, open vegetation, and the evolution of plants and animals during the Cenozoic. In E. Marinetto, E. Tschopp, & R. A. Gastaldo (Eds.), *Nature through time* (pp. 83–107). Springer Nature.

Schmidt, K. P. (1928). A new crocodile from New Guinea. *Field Museum of Natural History Zoological Series*, *12*, 176–181.

Shan, H.-Y., Wu, X.-C., Sato, T., Cheng, Y.-N., & Rufolo, S. (2021). A new alligatoroid (Eusuchia, Crocodylia) from the Eocene of China and its implications for the relationships of Orientalosuchina. *Journal of Paleontology*, *95*, 1321–1339.

Sherwood, R. J. (1999). Pneumatic processes in the temporal bone of chimpanzee (*Pan troglodytes*) and gorilla (*Gorilla gorilla*). *Journal of Morphology*, *241*, 127–137.

Shirley, M. H. (2010). Slender-snouted crocodile *Crocodylus cataphractus*. In S. C. Manolis & C. Stevenson (Eds.), *Crocodiles: Status survey and conservation action plan* (3rd ed., pp. 54–58). Crocodile Specialist Group.

Shirley, M. H., Oduro, W., & Beibro, H. Y. (2009). Conservation status of crocodiles in Ghana and Côte-d'Ivoire, West Africa. *Oryx*, *43*, 136–145.

Shirley, M. H., Vliet, K. A., Carr, A. N., & Austin, J. D. (2014). Rigorous approaches to species delimitation have significant implications for African crocodilian systematics and conservation. *Proceedings of the Royal Society of London B*, *281*, 20132483.

Smolensky, N. L. (2015). Co-occurring cryptic species pose challenges for conservation: A case study of the African dwarf crocodile (*Osteolaemus* spp.) in Cameroon. *Oryx*, *49*, 584–590.

Somaweera, R., Brien, M. L., Platt, S. G., Manolis, S. C., & Webber, B. L. (2019). Direct and indirect interactions with vegetation shape crocodylian ecology at multiple scales. *Freshwater Biology*, *64*, 257–268.

Storrs, G. W. (2003). Late Miocene-early Pliocene crocodilian fauna of Lothagam, Southwest Turkana Basin, Kenya. In M. G. Leakey & J. M. Harris (Eds.), *Lothagam: The Dawn of humanity in eastern Africa* (pp. 137–159). Columbia University Press.

Swofford, D. L. (2002). *PAUP*. Phylogenetic analysis using parsimony (*and other methods)* (4th ed.). Sinauer Associates.

Taylor, M. P., & Wedel, M. J. (in review). Why is vertebral pneumaticity in sauropod dinosaurs so variable? Qeios.

Tchernov, E. (1986). *Evolution of the crocodiles in east and North Africa*. CNRS.

Tchernov, E., & Couvering, J. V. (1978). New crocodiles from the early Miocene of Kenya. *Palaeontology*, *21*, 857–867.

Thorbjarnarson, J., & Wang, X. (2010). *The Chinese alligator: Ecology, behavior, conservation, and culture*. Johns Hopkins University Press.

Thorbjarnarson, J. B. (1996). Reproductive characteristics of the order Crocodylia. *Herpetologica*, *52*, 8–24.

Van Couvering, J. A., & Delson, E. (2020). African land mammal ages. *Journal of Vertebrate Paleontology*, *40*, e1803340.

Vashistha, G., Mungi, N. A., Lang, J. W., Ranjan, V., Dhakate, P. M., Khudsar, F. A., & Kothamasi, D. (2021). Gharial nesting in a reservoir is limited by reduced river flow and by increased bank vegetation. *Scientific Reports*, *11*, 4805.

Waitkuwait, W. E. (1986). Present knowledge of the west African slender-snouted crocodile, *Crocodylus cataphractus* Cuvier, 1824, and the west African dwarf crocodile *Osteolaemus tetraspis* Cope 1861. In P. Hall & R. Bryant (Eds.), *Crocodiles: Their ecology, management and conservation* (pp. 260–275). International Union for the Conservation of Nature.

Wang, Y.-Y., Sullivan, C., & Liu, J. (2016). Taxonomic revision of *Eoalligator* (Crocodylia, Brevirostres) and the paleogeographic origins of the Chinese alligatoroids. *PeerJ*, *4*, e2356.

Watkins, B. T. (2004). Reconstruction of the depositional environment of the middle Miocene primate locality, Maboko Island, Kenya. *Acta Mineralogica-Petrographica Abstract Series*, *4*, 113.

Webb, G. E., Messel, H., & Magnusson, W. E. (1977). The nesting of *Crocodylus porosus* in Arnhem Land, northern Australia. *Copeia*, *1977*, 238–249.

Webb, G. J. W., Buckworth, R., & Manolis, S. C. (1983). *Crocodylus johnstoni* in the McKinlay River, N.T. VI. Nesting biology. *Australian Wildlife Research*, *10*, 607–637.

Wedel, M. J., & Taylor, M. P. (2013). Caudal pneumaticity and pneumatic hiatuses in the sauropod dinosaurs *Giraffatitan* and *Apatosaurus*. *PLoS One*, *8*, e78213.

Westerhold, T., Marwan, N., Drury, A. J., Liebrand, D., Agnini, C., Anagnostou, E., Barnet, J. S. K., Bohaty, S. M., De Vleeschouwer, D., Florindo, F., Frederichs, T., Hodell, D. A., Holbourn, A. E., Kroon, D., Lauretano, V., Littler, K., Lourens, L. J., Lyle, M., Pälike, H., … Zachos, J. C. (2020). An astronomically dated record of Earth's climate and its predictability over the past 66 million years. *Science*, *369*, 1383–1387.

Wichura, H., Jacobs, L. L., Lin, A., Polcyn, M. J., Manthi, F. K., Winkler, D. A., Strecker, M. R., & Clemens, M. (2015). A 17-my-old whale constrains onset of uplift and climate change in East Africa. *Proceedings of the National Academy of Sciences of the United States of America*, *112*, 3910–3915.

Wilberg, E. (2017). Investigating patterns of crocodyliform cranial disparity through the Mesozoic and Cenozoic. *Zoological Journal of the Linnean Society*, *181*, 189–208.

Wu, X.-C., Li, C., & Wang, Y.-Y. (2018). Taxonomic assessment and phylogenetic test of *Asiatosuchus nanlingensis* Young, 1964 and *Eoalligator chunyii* Young, 1964. *Vertebrata PalAsiatica*, *56*, 137–146.

Young, C. C. (1964). New fossil crocodiles from China. *Vertebrata PalAsiatica*, *8*, 189–210.

Zangerl, R. (1944). *Brachyuranochampsa eversolei* gen. et sp. nov., a new crocodilian from the Washakie Eocene of Wyoming. *Annals of the Carnegie Museum*, *30*, 77–84.

Zhang, Z., Ramstein, G., Schuster, M., Li, C., Contoux, C., & Yan, Q. (2014). Aridification of the Sahara Desert caused by Tethys Sea shrinkage during the late Miocene. *Nature*, *513*, 401–404.

Zurriaguz, V., & Álvarez, A. (2014). Shape variation in presacral vertebrae of saltasaurine titanosaurs (Dinosauria, Sauropoda). *Historical Biology*, *26*, 801–809.

SUPPORTING INFORMATION

Additional supporting information may be found in the online version of the article at the publisher's website.